Int J Earth Sci (Geol Rundsch) (2017) 106:185–213
DOI 10.1007/s00531-016-1310-7

ORIGINAL PAPER

Petrogenesis and tectonic implications of the Neoproterozoic Datian mafic–ultramafic dykes in the Panzhihua area, western Yangtze Block, SW China

Yi-Jin Yang[1,2] · Wei-Guang Zhu[1] · Zhong-Jie Bai[1] · Hong Zhong[1] · Xian-Tao Ye[1] · Hong-Peng Fan[1]

Received: 2 August 2015 / Accepted: 21 February 2016 / Published online: 21 March 2016

Abstract Mafic–ultramafic dykes are important geological markers that can punctuate the onset of crustal extension during the breakup of a continent and provide valuable information on the mantle source. This study reports secondary ion mass spectroscopy zircon and baddeleyite U–Pb ages, elemental and Nd isotopic data for the Datian mafic–ultramafic dykes in the Panzhihua area, western Yangtze Block, SW China. Two kinds of rocks are confirmed: the picritic rock and the dolerite. Based on petrographic and geochemical features, the dolerite dykes are further subdivided into two groups: Group I mafic and Group II mafic dykes, which emplaced at ~760 Ma (zircon U–Pb) and ~800 Ma (zircon and baddeleyite U–Pb), respectively. All samples from the picritic rocks and the Group I mafic rocks show the features of high-Ti and alkaline basaltic magma in composition as well as "humped" trace element patterns, which are similar to those of typical alkaline basalts associated with continental rifts except for the slightly negative Nb–Ta anomalies. The Group II mafic rocks display the features of low-Ti and tholeiitic magma, moderately enriched in LILE and LREE, and characterized by distinctively negative Nb–Ta anomalies. The primary magmas of the picritic rocks and the Group I mafic rocks were generated from ca 25 % partial melting of an OIB-like, Nd isotopically depleted but incompatible elements relatively enriched mantle source within a garnet stable field. The Group II mafic rocks crystallized from crustal contaminated mafic magmas that were derived from a spinel-bearing sub-continental lithospheric mantle source, because of low ratios of La/Yb, Ti/Y and Sm/Yb. Geochemical features suggest that these groups of mafic–ultramafic dykes were formed in a continental rift setting, but derived from different mantle sources. In combination with other Neoproterozoic igneous rocks in the western margin of Yangtze Block, it is suggested that the Datian mafic–ultramafic dykes in the Panzhihua area could have been formed in a multistage continental rift system, most likely related to the proposed mantle superplume, which centered beneath South China at ca. 820 Ma and may have finally triggered the breakup of the supercontinent Rodinia.

Keywords Neoproterozoic · Mafic–ultramafic dykes · Geochemistry · Southwest China · Rodinia

Introduction

Recent studies on the various constituent fragments of the supercontinent Rodinia have made great progresses on the assembly and breakup of this supercontinent (Ernst et al. 2008; Li et al. 2008; Bogdanova et al. 2009; Evans 2013; Nance et al. 2014). South China, including the Yangtze and Cathaysia blocks, has been considered a key area for understanding the Neoproterozoic supercontinent Rodinia (Li et al. 1995, 2008; Zhou et al. 2002a, b, 2006; Zhao and Zhou 2007a, b). Neoproterozoic (Ca. 860–740 Ma) igneous rocks are widespread across the Yangtze Block. Research on these igneous rocks played an important role in the reconstruction of the supercontinent Rodinia and understanding the tectonic mechanism of South China Block during this period. Many of these igneous rocks have been

✉ Wei-Guang Zhu
zhuweiguang@vip.gyig.ac.cn

[1] State Key Laboratory of Ore Deposit Geochemistry, Institute of Geochemistry, Chinese Academy of Sciences, 99 West Lincheng Road, Guiyang 550081, China

[2] University of Chinese Academy of Sciences, Beijing 100049, China

studied during the recent decades, but the petrogenesis and tectonic implications of these igneous rocks are still controversial. Li and his co-authors considered these rocks were anorogenic products, which were concurrent with rapid continental-scale crustal doming and unroofing and the development of Nanhua and Kangdian rifts, related to mantle plume activities during the breakup of the supercontinent Rodinia (Li et al. 1999, 2002a, b, 2003a, b, 2006; Lin et al. 2007; Zhou et al. 2007). On the contrary, Zhou and others believed that these rocks were formed in an island arc environment (Zhou et al. 2002a, b; Zhao and Zhou 2007a, b; Zhao et al. 2008; Wang et al. 2013, 2014).

Mafic dykes are important geological time markers that usually punctuate the onset of crustal extension (Spaeth et al. 1995) and offer valuable information of the mantle source (Kullerud et al. 2006). The Neoproterozoic mafic dykes in the western margin of the Yangtze Block, in spite of their small volume, can provide important constraints on the tectonic setting of the South China and are also critical in testing the different tectonic models. Numerous Neoproterozoic mafic–ultramafic dykes intruded into the late Paleo- to Mesoproterozoic strata and Neoproterozoic granitic and dioritic intrusion in the Panzhihua area, Sichuan province, SW China (Fig. 1). In this study, precise SIMS U–Pb zircon and baddeleyite dating, and comprehensive elemental and Nd isotopic data are reported for the Datian mafic–ultramafic dykes in the Panzhihua area. The purposes of this study are to (1) determine the emplacement ages for the mafic–ultramafic dykes, (2) demonstrate the origin and petrogenesis of the mafic–ultramafic rocks, and (3) shed new lights on the Neoproterozoic magmatic and tectonic evolution of the western margin of the Yangtze Block, and on its relation to the supercontinent Rodinia.

Geological background and petrography

The western margin of Yangtze Block is to the east of the Songpan–Ganzi thrust belt (Fig. 1). The Songpan–Ganzi terrane is characterized by a thick (several to >10 km) sequence of late Triassic strata of deep marine origin that were deposited on oceanic crust. The metamorphic core complexes in this terrane were unroofed by nearly east–west extension in the Mesozoic (180–150 Ma) (Zhao and Zhou 2007a and the references therein). The basement in the western margin of the Yangtze Block mainly consists of late Paleoproterozoic to earliest Neoproterozoic metasedimentary rocks interbedded with felsic and mafic metavolcanic rocks, which are termed as the Dahongshan, Hekou, Kunyang, Huili and Yanbian Groups at different localities (Greentree et al. 2006; Li et al. 2006; Greentree and Li 2008; He 2009; Zhao 2010). Above the basement, a thick sequence (>9 km) of Late Neoproterozoic (820–540 Ma) to Permian strata consists of clastic, carbonate and metavolcanic rocks (Cong 1988; SBGMR 1991).

The Neoproterozoic igneous rocks are widely distributed along the western margin of the Yangtze Block, which include felsic intrusive and volcanic rocks as well as mafic–ultramafic rocks and intermediate rocks (e.g., Li et al. 2002a, 2003a, b, 2006; Zhou et al. 2002a, b, 2006). Commonly, the mafic rocks are closely associated with the felsic rocks in time and space. Neoproterozoic igneous complexes are well preserved, including the Kangding, Miyi, Tongde, Datian and Yuanmou Complexs from north to south (Zhou et al. 2002a; Li et al. 2003b). Neoproterozoic mafic and ultramafic intrusions, such as the ca. 825 Ma Gaojiacun and ca. 821 Ma Lengshuiqing plutons (Zhu et al. 2006, 2007), ca. 752 Ma Shaba pluton (Li et al. 2003b) and ca. 740 Ma Dadukou pluton (Zhao and Zhou 2007b), crop out throughout the western margin of the Yangtze Block.

The Datian mafic–ultramafic dykes are located in the Panzhihua area, and from north to south intruded into the Datian quartz dioritic pluton (760 ± 4 Ma, Zhao and Zhou 2007a), the Datian Formation of the Huili Group and the Heime granitic pluton (Fig. 1). The Datian formation is divided into two sections: the lower section and the upper section. The lower section mainly contains granitic migmatite and gneiss, whereas the upper section consists of amphibolite and migmatite. During the 1:200,000 regional geological survey of People's Republic of China, the Heime granodiorite was considered to be product of the "Jinning magmatism" (YBG 1972).

The Datian mafic–ultramafic dykes are commonly 1–5 m wide, and their lengths are unclear. The orientations of the mafic–ultramafic dykes are relatively variable, varying from northeast to east in strikes and from 20° to 50° in dips to the NW. Based on different lithologies, two kinds of rocks (dykes) are classified: picritic rock and dolerite. Due to the limited outcrops of these mafic–ultramafic dykes, it is hard to judge whether cross-cutting relationship exists between the picritic dyke and dolerite dykes.

For the picritic rocks, only one picritic dyke crop out and it intruded into the Huili Group in the area (Fig. 1). They are composed of olivine (30–40 % by volume), clinopyroxene (30–40 %), hornblende (20–30 %), Fe–Ti oxide (2–4 %) and chromite (<1 %). The picritic rocks are phyric in texture and contain abundant (30–50 %) large phenocrysts of olivine and clinopyroxene. The matrix minerals consist mainly of clinopyroxene and hornblende. Olivine (30–40 % by volume) only shows pseudomorphs due to the intensive serpentinization (Fig. 2a, b). Euhedral chromite grains are enclosed in olivine, and the early crystallized clinopyroxene is normally surrounded by later formed anhedral hornblende (Fig. 2a, b).

The dolerite dykes, showing distinctive feature of occurrence, mineral assemblage, emplacement age and

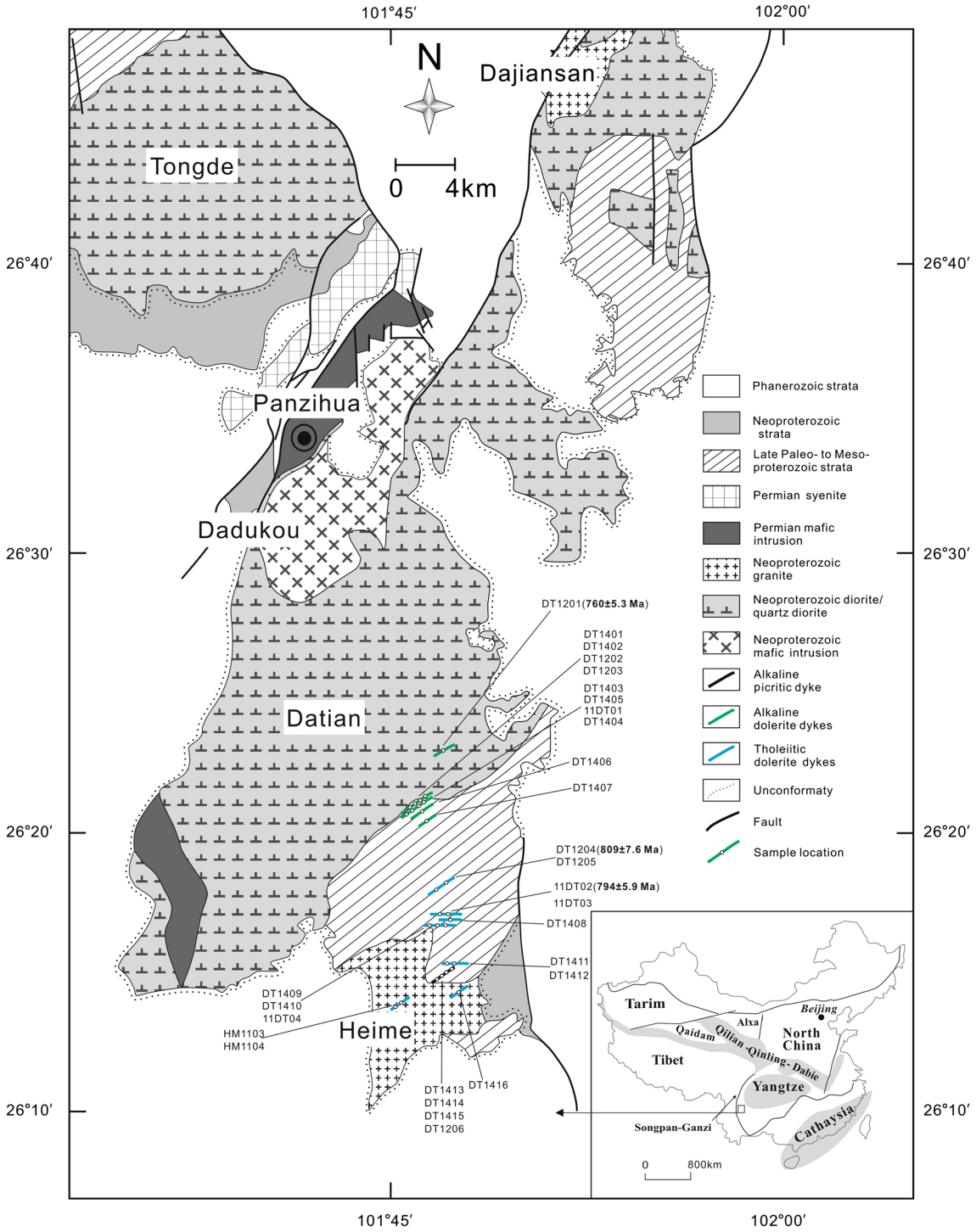

Fig. 1 Simplified geological map of the Panzhihua area, Sichuan province, SW China (modified after YBG 1972; Zhao and Zhou 2007a)

geochemical compositions, can be further divided into two groups. No cross-cutting relations between the two groups are observed. One group (Group I) of dolerite dykes shows intruding contacts with the Datian quartz diorite pluton and the Huili Group. Such rocks are moderately altered, dark-gray, fine-grained in texture (Fig. 2c, d). Alteration is dominated by argilation, chloritization, and amphibolization. Moreover, many clinopyroxenes have been altered to hornblende (Fig. 2c, d). These mafic rocks are composed of plagioclase (40–50 % in volume), hornblende (20–40 %), clinopyroxene (5–10 %), biotite (1–2 %) and Fe–Ti oxide (1–2 %). They are formed at

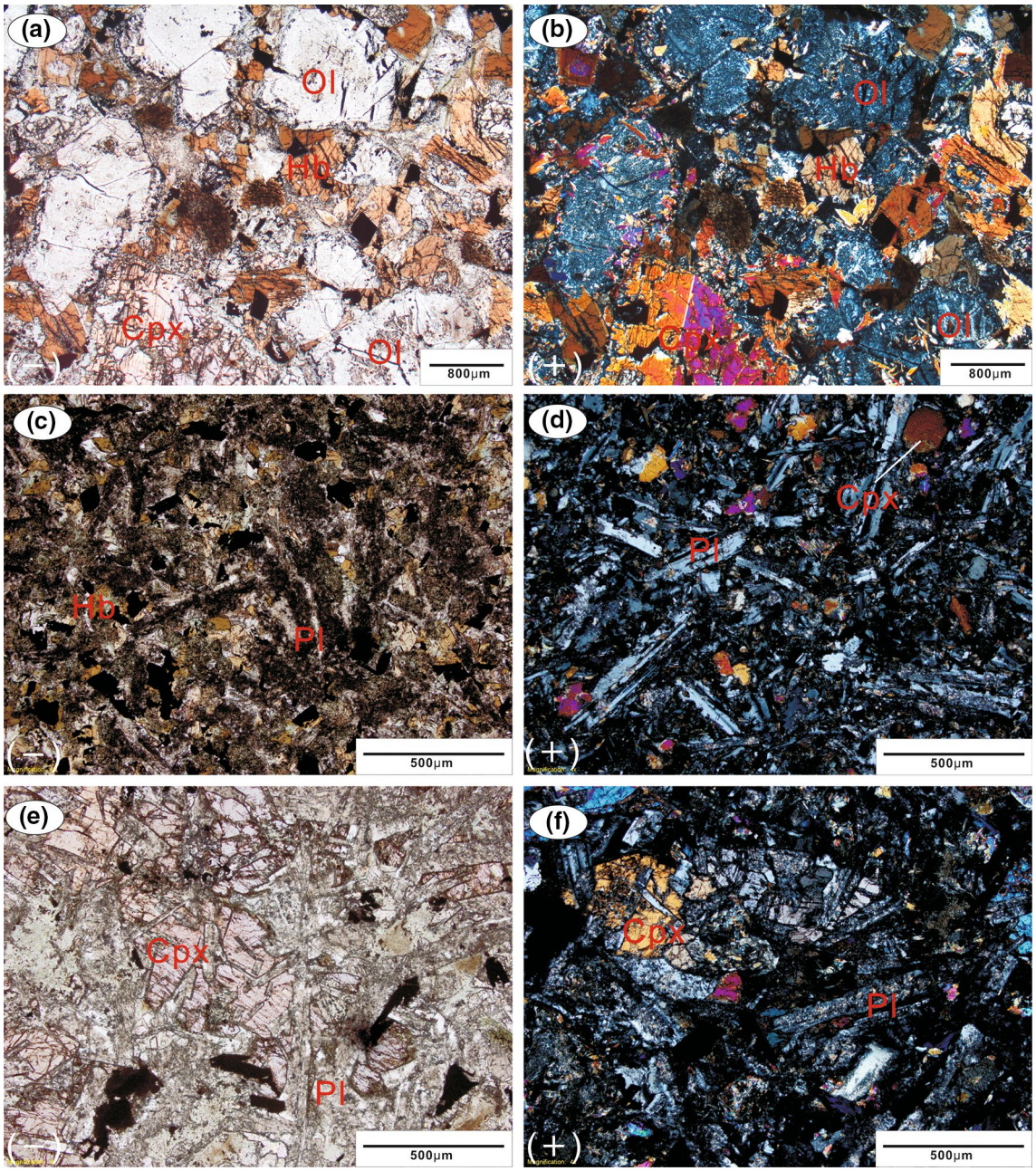

Fig. 2 Photomicrographs of the representative Datian mafic–ultramafic dykes in the Panzhihua area. The picritic dyke (**a**, **b**), the Group I mafic dykes (**c**, **d**), and the Group II mafic dykes (**e**, **f**)

ca. 760 Ma and belong to alkaline basalts (see details in "Results" section). On the contrary, the Group II dolerite dykes intruded into the Huili Group and Heime granite pluton to the north of the dolerite dykes stated above. This type of dolerite rocks are slightly to moderately alterated, dark-gray to dark and have typical diabasic texture, in which xenomorphic clinopyroxene and Fe–Ti oxides fill into the spaces between the semi- to euhedral plagioclase (Fig. 2e, f). Alteration also includes argilation, chloritization, and amphibolization, but the clinopyroxenes are relatively fresh. Mineral grains in these dolerite rocks are coarser than that of the former group (Fig. 2). Rock-forming minerals in the Group II dolerite dykes include plagioclase (40–55 % in volume), clinopyroxene (10–40 %), hornblende (5–25 %), biotite (1–2 %), and Fe–Ti oxide (1–2 %). They are formed at ca. 800 Ma and belong to tholeiitic basalts (see details in "Results" section). For the convenience of description, the former

group of dolerite dykes is defined as Group I mafic dykes and the latter as Group II mafic dykes.

Analytical methods

Three samples were collected for U–Pb dating, including sample DT1201 (zircon) from the Group I mafic dykes, and sample 11DT02 (baddeleyite) and sample DT1204 (zircon) from the Group II mafic dykes, respectively. Zircon and baddeleyite grains were separated using conventional heavy liquid and magnetic techniques. Representative zircon and baddeleyite grains were handpicked under a binocular microscope and mounted in an epoxy resin disk, and then polished with high-purity gold film. Zircon and baddeleyite were imaged with transmitted and reflected light micrographs as well as cathodoluminescence (CL) images and backscattered electron images to reveal their external and internal structures. Measurements of U, Th and Pb for samples 11DT02, DT1201 and DT1204 were conducted using a Cameca SIMS-1280 ion microprobe at the Institute of Geology and Geophysics, Chinese Academy of Sciences, Beijing. Details of the analytical procedures for zircon and baddeleyite U–Pb dating can be found in Li et al. (2009, 2010), respectively. Oxygen flood that introduces oxygen into the sample chamber was used during the analyses, which not only enhances Pb^+ ion yield by a factor of 2 and 7 for zircon and baddeleyite (Li et al. 2009, 2010), respectively, but also depresses the U–Pb orientation effect (Wingate and Compston 2000) down to ~2 % (Li et al. 2010). All baddeleyites were mounted in random orientations due to their small sizes and polysynthetic twinning. The analytical results are presented in Table 1. The uncertainties in ages are cited as 1σ, and the weighted mean ages are quoted at the 95 % confidence interval (2σ).

Major element compositions of whole rocks were determined using X-ray fluorescence spectrometers (XRF) at the ALS Chemex Co Ltd, Guangzhou. The analytical precision was better than 5 %. Trace elements in whole rocks were analyzed using a Perkin-Elmer Sciex ELAN DRC-e ICP–MS at the State Key Laboratory of Ore Deposit Geochemistry (SKLODG), Institute of Geochemistry, Chinese Academy of Sciences (IGCAS). The powdered samples (50 mg) were dissolved with HF + HNO_3 mixture in high-pressure Teflon bombs at ~190 °C for 48 h (Qi et al. 2000). Rh was used as an internal standard to monitor signal drift during measurement. The international standards GBPG-1 and OU-6, and the Chinese National standards GSR-1 and GSR-3 were used for analytical quality control. The analytical precision was generally better than 10 % for trace elements.

Chemical compositions of clinopyroxene were determined by wavelength-dispersion X-ray emission spectrometry using an EPMA-1600 electron microprobe at the SKLODG, IGCAS. Accelerating voltage is 25 kV, a beam current of 10 nA and a spot diameter of 10 μm were used. The detection limit for these elements under such conditions is 0.01 wt%, and analytical reproducibility was within 2 %.

Samples for Nd isotopic analysis were spiked and dissolved with HF + HNO_3 acid in Teflon bombs. Sm and Nd were separated by conventional cation-exchange techniques. The isotopic measurements were performed on a thermal ionization mass spectrometry (TIMS)—Triton at the SKLODG and a Nu Plasma muticollector mass spectrometer (MC–ICP–MS) at the State Key Laboratory of Environmental Geochemistry (SKLEG), IGCAS. The measured $^{143}Nd/^{144}Nd$ ratios were normalized to $^{146}Nd/^{144}Nd = 0.7219$. The $^{143}Nd/^{144}Nd$ ratios of the USGS standard rock BCR-2 determined during this study were 0.512655 ± 6 (2σ) and 0.512659 ± 6 (2σ), for TIMS and MC–ICP–MS, respectively.

Results

U–Pb zircon and baddeleyite geochronology

Zircon ages for samples DT1201 and DT1204

Sample DT1201 (N26°22′55.6″, E101°46′58.7″) and sample DT1204 (N26°18′02.3″, E101°46′51.5″) are selected from the Groups I and II mafic rocks, respectively. Zircon grains from sample DT1201 are generally transparent, euhedral prismatic with simple internal growth zoning (Fig. 3a), characteristic of magmatic zircons. They have maximum length up to 200 μm with length-to-width ratios of 1:1 to 1:2 (Fig. 3a). Fourteen analyses were obtained from 14 grains during a single analytical session. Measured U concentrations vary from 98 to 216 ppm, and Th concentrations range from 75 to 200 ppm, with Th/U ratios of 0.52 to 1.05 (Table 1). All 14 analyses measured $^{206}Pb/^{238}U$ ages are in good agreement within analytical errors, yielding a weighted age of 760 ± 5.3 Ma (Fig. 4a). This age is considered as the best estimate of the crystallization age for sample DT1201.

In sample DT1204, zircon grains are transparent with length of 50–150 μm and length-to-width ratios of 1:1 to 1:2. In CL images, most zircon grains show no obvious structure, but a few show simple internal growth zoning (Fig. 3b), which implies a magmatic origin. Fourteen analyses were obtained from 14 grains during a single analytical session. Measured U concentrations for these zircon grains vary from 37 to 281 ppm and measured Th concentrations from 11 to 168 ppm, with Th/U ratios range from 0.23 to 0.64 (Table 1). All the analyses are concordant in U–Pb and

Table 1 Cameca SIMS zircon and baddeleyite U–Pb isotopic analyses for the Datian mafic–ultramafic dykes in the Panzhihua area, SW China

Sample spot #	U (ppm)	Th (ppm)	Th/U	$^{206}Pb/^{204}Pb$ measured	f_{206} (%)	Isotopic ratio						Age/Ma	
						$^{207}Pb^*/^{206}Pb^*$	$\pm1\sigma$ (%)	$^{207}Pb^*/^{235}U$	$\pm1\sigma$ (%)	$^{206}Pb^*/^{238}U$	$\pm1\sigma$ (%)	$^{206}Pb^*/^{238}U \pm 1\sigma$	$^{207}Pb^*/^{206}Pb^* \pm 1\sigma$
DT1201 zircon (N 26°22′55.6″, E 101°46′58.7″)													
1	98	75	0.763	7819	0.24	0.06467	1.02	1.12144	1.83	0.1258	1.52	764 ± 11	764 ± 21
2	178	143	0.808	14,159	0.13	0.06475	0.76	1.11896	1.68	0.1253	1.50	761 ± 11	766 ± 16
3	191	182	0.953	23,279	0.08	0.06475	0.79	1.11255	1.69	0.1246	1.50	757 ± 11	766 ± 16
4	187	97	0.520	32,000	0.06	0.06512	0.86	1.12745	1.73	0.1256	1.50	763 ± 11	778 ± 18
5	152	122	0.802	18,640	0.10	0.06459	1.31	1.11789	1.99	0.1255	1.50	762 ± 11	761 ± 27
6	114	76	0.665	7271	0.26	0.06498	1.04	1.11568	1.82	0.1245	1.50	757 ± 11	774 ± 22
7	180	145	0.807	1160	1.61	0.06460	1.89	0.95927	2.44	0.1077	1.54	659 ± 10	761 ± 39
8	211	136	0.646	19,019	0.10	0.06436	0.69	1.11733	1.66	0.1259	1.51	765 ± 11	753 ± 15
9	167	114	0.682	25,907	0.07	0.06460	1.03	1.10344	1.82	0.1239	1.50	753 ± 11	761 ± 21
10	194	140	0.721	11,123	0.17	0.06448	1.21	1.10177	1.93	0.1239	1.50	753 ± 11	757 ± 25
11	211	200	0.949	7326	0.26	0.06429	0.83	1.10068	1.71	0.1242	1.50	755 ± 11	751 ± 17
12	216	169	0.780	27,074	0.07	0.06480	0.81	1.11975	1.71	0.1253	1.50	761 ± 11	768 ± 17
13	152	108	0.712	8708	0.21	0.06523	0.97	1.12321	1.81	0.1249	1.52	759 ± 11	782 ± 20
14	148	155	1.049	321,657	0.01	0.06462	1.49	1.11294	2.14	0.1249	1.53	759 ± 11	762 ± 31
DT1204 zircon (N 26°18′02.3″, E 101°46′51.5″)													
1	102	44	0.434	n/a	0.00	0.06704	1.74	1.20887	2.33	0.1308	1.55	792 ± 12	839 ± 36
2	222	143	0.644	67,933	0.03	0.06515	1.07	1.19285	1.90	0.1328	1.57	804 ± 12	779 ± 22
3	71	29	0.405	20,983	0.09	0.06577	2.67	1.19401	3.07	0.1317	1.50	797 ± 11	799 ± 55
4	75	33	0.434	22,851	0.08	0.06472	1.86	1.17907	2.45	0.1321	1.60	800 ± 12	765 ± 39
5	94	31	0.324	n/a	0.00	0.06476	1.81	1.18630	2.35	0.1329	1.50	804 ± 11	767 ± 38
6	84	45	0.539	41,856	0.04	0.06557	1.75	1.20217	2.31	0.1330	1.52	805 ± 11	793 ± 36
7	66	21	0.319	n/a	0.00	0.06747	1.97	1.21387	2.50	0.1305	1.54	791 ± 11	852 ± 40
8	90	48	0.535	9225	0.20	0.06551	3.10	1.17186	3.45	0.1297	1.52	786 ± 11	791 ± 64
9	281	168	0.597	144,633	0.01	0.06661	1.08	1.20985	1.85	0.1317	1.51	798 ± 11	826 ± 22
10	56	13	0.225	104,889	0.02	0.06703	2.18	1.19933	2.65	0.1298	1.50	787 ± 11	839 ± 45
11	63	24	0.379	18,319	0.10	0.06564	2.26	1.18678	2.71	0.1311	1.50	794 ± 11	795 ± 47
12	37	14	0.386	18,961	0.10	0.06728	2.82	1.19602	3.19	0.1289	1.50	782 ± 11	846 ± 58
13	108	44	0.410	189,716	0.01	0.06654	2.45	1.19189	2.88	0.1299	1.50	787 ± 11	823 ± 50
14	41	11	0.283	27,622	0.07	0.06625	2.77	1.16586	3.15	0.1276	1.50	774 ± 11	814 ± 57
11DT02 baddeleyite (N 26°17′06.6″, E 101°46′59.5″)													
1	452	14	0.032	224,964	0.01	0.06671	0.53	1.18827	3.08	0.1292	3.03	783 ± 22	829 ± 11
2	415	2	0.004	n/a	0.00	0.06544	0.60	1.08939	3.09	0.1207	3.03	735 ± 21	789 ± 13
3	945	63	0.066	619,637	0.00	0.06674	1.04	1.08065	3.21	0.1174	3.04	716 ± 21	830 ± 22

Table 1 continued

Sample spot #	U (ppm)	Th (ppm)	Th/U	$^{206}Pb/^{204}Pb$ measured	f_{206} (%)	Isotopic ratio						Age/Ma	
						$^{207}Pb^*/^{206}Pb^*$	$\pm 1\sigma$ (%)	$^{207}Pb^*/^{235}U$	$\pm 1\sigma$ (%)	$^{206}Pb^*/^{238}U$	$\pm 1\sigma$ (%)	$^{206}Pb^*/^{238}U \pm 1\sigma$	$^{207}Pb^*/^{206}Pb^* \pm 1\sigma$
4	342	3	0.008	n/a	0.00	0.06591	0.63	1.11965	3.11	0.1232	3.04	749 ± 22	804 ± 13
5	204	4	0.018	458,861	0.00	0.06582	0.82	1.16033	3.19	0.1279	3.09	776 ± 23	801 ± 17
6	175	1	0.003	n/a	0.00	0.06645	0.88	1.14770	3.18	0.1253	3.05	761 ± 22	821 ± 18
7	1814	39	0.021	714,603	0.00	0.06596	0.37	1.16581	3.05	0.1282	3.03	778 ± 22	805 ± 8
8	140	4	0.026	17,551	0.11	0.06600	1.15	1.19879	3.24	0.1317	3.03	798 ± 23	806 ± 24
9	119	1	0.006	25,700	0.07	0.06527	1.76	1.12203	3.53	0.1247	3.06	757 ± 22	783 ± 37
10	426	16	0.037	235,237	0.01	0.06675	0.56	1.27061	3.11	0.1381	3.06	834 ± 24	830 ± 12
11	221	1	0.003	n/a	0.00	0.06604	0.74	1.12721	3.13	0.1238	3.05	752 ± 22	808 ± 15
12	265	1	0.004	240,030	0.01	0.06548	0.81	1.08204	3.34	0.1199	3.24	730 ± 22	790 ± 17
13	408	8	0.020	n/a	0.00	0.06678	0.56	1.19757	3.10	0.1301	3.05	788 ± 23	831 ± 12
14	388	15	0.039	n/a	0.00	0.06553	0.64	1.18887	3.11	0.1316	3.05	797 ± 23	791 ± 13
15	609	12	0.019	5396	0.35	0.06830	1.25	1.37965	3.33	0.1465	3.09	881 ± 26	878 ± 26
16	210	0	0.002	569,344	0.00	0.06565	0.96	1.11958	3.27	0.1237	3.12	752 ± 22	795 ± 20
17	476	14	0.030	n/a	0.00	0.06666	0.70	1.25526	3.12	0.1366	3.04	825 ± 24	827 ± 15
18	516	3	0.007	473,753	0.00	0.06537	0.51	1.20683	3.19	0.1339	3.15	810 ± 24	786 ± 11
19	888	26	0.029	990,78	0.02	0.06631	0.46	1.26157	3.09	0.1380	3.05	833 ± 24	816 ± 10
20	434	13	0.031	180,001	0.01	0.06584	0.65	1.21434	3.11	0.1338	3.05	809 ± 23	801 ± 14

Errors are 1σ; f_{206} is the percentage of common ^{206}Pb in total ^{206}Pb; common Pb corrected using the measured ^{204}Pb

n/a Not available

* Indicates the radiogenic ^{207}Pb and ^{206}Pb

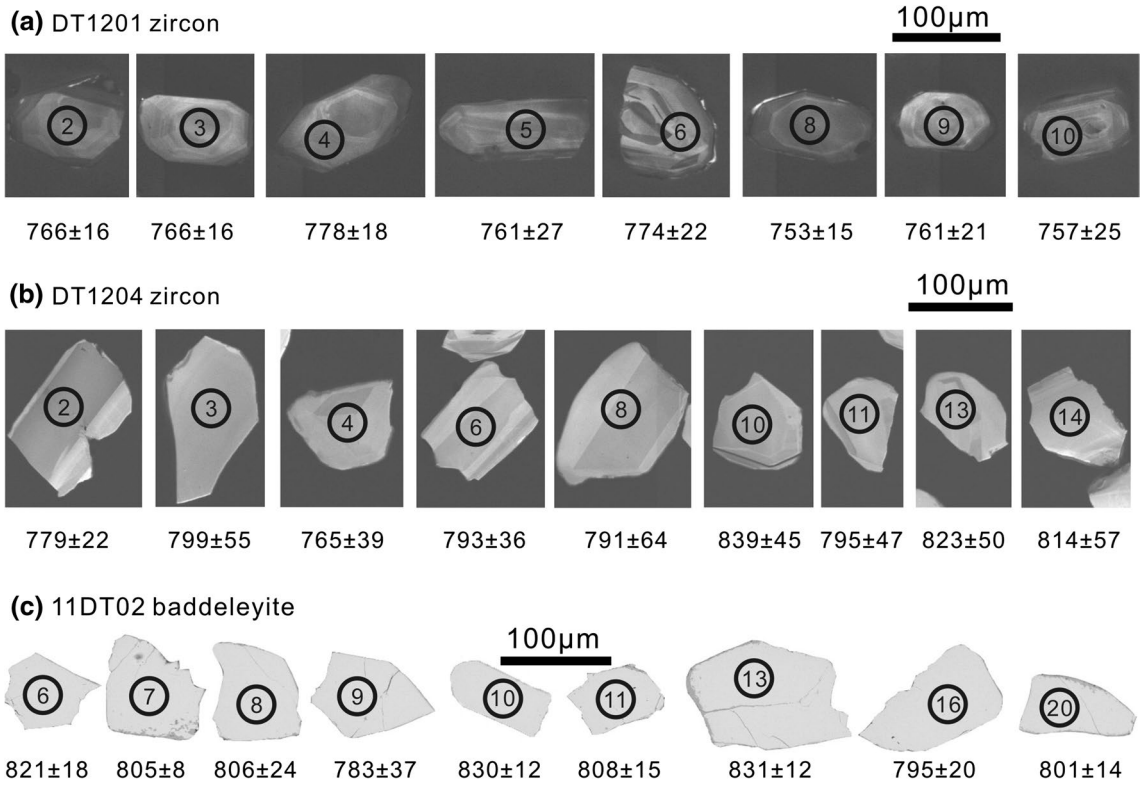

Fig. 3 Transmitted CL images of representative zircons from sample DT1201 (**a**) and DT1204 (**b**), and backscattered electron images of baddeleyites from sample 11DT02 (**c**) $^{207}Pb/^{206}Pb$ ages for the spots on representative grains are shown in Ma with 1σ errors

Pb–Pb isotopes within analytical errors, and the weighted mean of $^{206}Pb/^{238}U$ yields an age of 794 ± 5.9 Ma (2σ) (Fig. 4b), which can be considered to represent the formation age of sample DT1204.

Baddeleyite age for sample 11DT02

Sample 11DT02 (N26°17′06.6″, E101°46′59.5″) is dolerite collected from the Group II mafic dykes. The baddeleyite grains in the sample are mostly anhedral, ranging from 50 to 150 μm in length, and have length-to-width ratios between 1:1 and 2:1 (Fig. 3c). Twenty analyses were conducted on 20 grains during a single analytical session. Uranium concentrations are between 119 and 1814 ppm, and thorium contents range from 1 to 63 ppm, with Th/U ratios of 0.003–0.039 (Table 1). All the 20 analyses give near-concordant U–Pb results (Fig. 4c). The weighted mean $^{207}Pb/^{206}Pb$ age is 809 ± 7.6 Ma (95 % confidence interval, MSWD = 1.4), which is interpreted as the best estimate of the crystallization age for sample 11DT02. This age, consistent with the zircon U–Pb age of DT1204 (794 ± 5.9 Ma), suggests that the age of ~800 Ma represents the formation age for the Group II mafic rocks.

Mineral chemistry

The electron microprobe analyses of representative clinopyroxene are listed in "Appendix." Electron microprobe analysis indicates that the compositions of clinopyroxenes from the Group I mafic rocks and the picritic rocks are $Wo_{35–43}$ $En_{41–52}$ $Fs_{11–20}$ and $Wo_{43–48}$ $En_{43–48}$ $Fs_{5–11}$, respectively. The former belongs to augite exclusively with $Mg^{\#}$ ranging from 69 to 82, but the latter mainly belongs to diopside with $Mg^{\#}$ of 80–89 ("Appendix"). The compositions of clinopyroxene from the Group II mafic rocks are $Wo_{35–48}$ $En_{34–39}$ $Fs_{13–25}$, which belong to diopside and augite with $Mg^{\#}$ of 57–73 ("Appendix").

Elemental geochemistry

Major and trace element compositions for the twenty-six samples are presented in Table 2. All the samples in this study have experienced varying degrees of alteration, which is shown by the different loss on ignition (LOI) values of 0.65–5.2 wt%. During alteration, the mobile elements, such as K and Na, and large-ion lithophile elements (LILE: Cs, Rb, Sr, Ba, etc.) could be removed easily from the rocks by fluids, but the immobile elements, such as

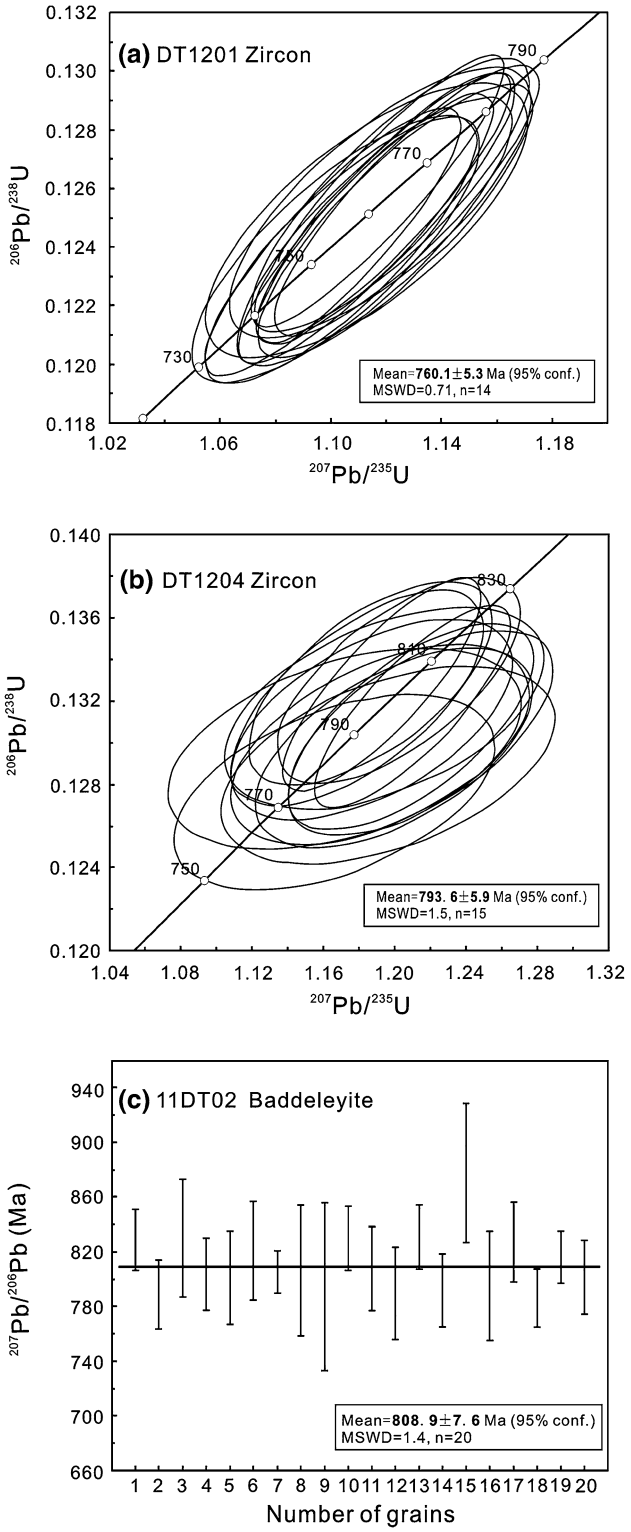

Fig. 4 SIMS zircon U–Pb concordia diagrams of sample **a** DT1201 and **b** DT1204. SIMS weighted mean $^{207}Pb/^{206}Pb$ ages on 20 baddeleyite grains of sample 11DT02, and the *error bars* represent 95 % confidence limits of measurements (**c**)

rare earth elements (REE) and high-field strength elements (HFSE: Ti, Zr, Y, Nb, Ta, Hf, etc.) were removed by fluids difficultly. Therefore, these immobile elements can be used for petrochemical classification and petrogenetic discussion. The sums of major element oxides of all samples are recalculated to 100 % volatile free.

Geochemical characteristics of the picritic dyke

The picritic dyke is picritic in composition with SiO_2 ranging from 44.9 to 45.5 wt% (volatile-free). In addition, the picritic rocks have high MgO (22.8–23.8 wt%), Fe_2O_3 (14.5–14.7 wt%), Cr (1957–2260 ppm), Ni contents (726–1464 ppm) and $Mg^{\#}$ values (75.7–76.3). In the chondrite-normalized REE diagram (Fig. 5a), these rocks show obviously LREE-enriched and HREE-depleted patterns with La_N (the subscript N denotes chondrite-normalized) values of 51–56, $(La/Yb)_N$ ratios of 8.4–12.1, $(La/Sm)_N$ ratios of 2.5–3.1 and $(Gd/Yb)_N$ ratios of 2.5–3.1. Moreover, the picritic rocks display no distinctive Eu anomalies (Fig. 5a) with the δEu values ranging from 0.88 to 1.0. In the primitive mantle-normalized spider diagram (Fig. 5b), all picritic rocks are characterized by "humped" patterns, broadly similar to those of the Suxiong alkaline basalts (Li et al. 2002a) and ocean island basalt (OIB) provinces (Sun and McDonough 1989). As shown in Fig. 5b, the picritic rocks display slightly negative to insignificant Nb–Ta anomalies [$(Nb/La)_P = 0.83$–0.94; the subscript P denotes primitive mantle-normalized], obvious negative Sr anomalies and positive Ti anomalies.

Geochemical characteristics of the dolerite dykes

The Groups I and II dolerite dykes are both basaltic rocks in composition with SiO_2 contents ranging from 47.8 to 50.1 and 47.3 to 53.3 wt% (volatile-free), respectively. The Group I mafic rocks contain MgO from 6.4 to 9.8 wt%, Fe_2O_3 from 12.4 to 13.9 wt%, TiO_2 from 2.0 to 2.6 wt%, $Mg^{\#}$ from 50.2 to 61.2, Cr from 64 to 614 ppm and Ni from 47 to 260 ppm. Although the Group II mafic rocks have similar major elements compositions to that of Group I mafic rocks, larger variations are obvious with MgO from 5.2 to 9.7 wt%, Fe_2O_3 from 9.3 to 16.9 wt%, TiO_2 from 0.31 to 3.7 wt%, $Mg^{\#}$ from 37.8 to 64.1, Cr from 97 to 881 ppm and Ni from 6.97 to 171 ppm.

Similar to the picritic rocks, the Group I mafic rocks display obviously LREE-enriched and HREE-depleted patterns in the chondrite-normalized REE diagram (Fig. 5a) with La_N values of 71–115, $(La/Yb)_N$ ratios of 8.3–12.9, $(La/Sm)_N$ ratios of 2.5–3.6 and $(Gd/Yb)_N$ ratios of 2.1–2.8. Different from Group I mafic rocks, the Group II mafic

Table 2 Major element (in wt%) and trace element (in ppm) compositions of the Datian mafic–ultramafic dykes in the Panzhihua area, SW China

Sample	DT1206	DT1413	DT1414	DT1415	11DT01	DT1201	DT1202	DT1203	DT1401	DT1402
Group	Pic	Pic	Pic	Pic	I	I	I	I	I	I
Major elements (wt%)										
SiO_2	42.27	42.70	42.20	43.00	48.66	46.48	47.95	48.13	48.30	47.90
TiO_2	1.73	1.77	1.76	1.82	2.40	2.56	2.27	2.29	2.29	2.26
Al_2O_3	4.96	5.06	5.00	5.25	14.01	12.16	13.55	13.66	13.70	13.60
Fe_2O_3	13.76	13.74	13.76	13.76	12.24	13.55	12.30	12.22	12.34	12.30
MnO	0.18	0.18	0.18	0.17	0.18	0.17	0.18	0.18	0.18	0.18
MgO	22.40	21.80	21.90	21.60	6.23	8.65	6.90	6.84	6.74	6.66
CaO	7.92	8.28	7.85	7.94	9.59	9.95	10.16	9.86	9.92	9.51
Na_2O	0.60	0.61	0.62	0.65	2.65	2.59	2.53	2.71	2.56	2.48
K2O	0.22	0.23	0.22	0.21	1.15	0.85	1.00	1.24	1.03	1.08
P_2O_5	0.16	0.16	0.16	0.16	0.25	0.30	0.25	0.27	0.25	0.25
LOI	5.21	4.60	4.80	4.34	1.87	2.28	2.41	2.24	2.30	2.14
Total	99.41	99.13	98.45	98.90	99.24	99.54	99.50	99.64	99.61	98.36
$Mg^{\#}$	76.3	75.9	75.9	75.7	50.2	55.8	52.6	52.6	52.0	51.8
Trace elements (ppm)										
Sc	11.3	35.7	33.9	35.1	27.7	33.0	29.6	29.2	36.7	36.8
V	191	245	236	238	230	236	239	238	314	314
Cr	1957	2260	2230	2170	64	267	101	99	108	108
Co	119	115	118	117	48.6	51.1	48.3	47.5	47.6	47.9
Ni	726	1337	1465	1313	46.8	140	91.0	82.9	114	116
Cu	81.7	129	117	116	96.1	115	139	123	185	152
Zn	165	148	147	135	174	159	132	149	114	118
Ga	9.64	9.87	9.72	9.78	19.7	18.4	19.6	19.7	20.2	20.4
Rb	8.69	8.48	7.29	4.80	36.4	23.4	35.2	41.2	33.6	32.7
Sr	168	170	173	172	576	535	546	515	593	560
Y	15.3	15.8	12.7	12.2	23.2	24.1	23.1	23.0	23.7	23.6
Zr	87.7	93.4	91.4	98.9	183	215	186	186	188	191
Nb	15.4	15.0	14.5	15.4	29.4	30.2	27.9	28.9	26.9	26.5
Cs	2.87	2.79	2.63	1.47	0.53	0.14	0.37	0.69	0.39	0.30
Ba	594	650	603	148	673	641	310	379	451	346
La	17.5	17.3	16.0	15.7	35.6	30.7	31.1	32.2	32.1	31.9
Ce	32.7	35.2	34.6	35.3	71.6	65.1	64.3	66.3	68.6	68.6
Pr	4.94	4.50	4.41	4.24	8.16	8.85	8.06	8.38	7.90	8.15
Nd	20.5	18.2	18.0	17.4	31.8	34.8	31.0	32.4	32.5	31.9
Sm	4.46	3.55	3.70	3.68	6.19	7.65	6.52	6.44	6.15	6.13
Eu	1.47	1.16	1.13	1.02	1.93	2.45	2.08	2.11	2.10	1.93
Gd	4.54	3.41	3.60	3.38	6.15	6.94	6.30	6.56	5.95	5.23
Tb	0.69	0.54	0.49	0.49	0.84	1.06	0.93	0.95	0.87	0.85
Dy	3.40	2.84	2.78	2.43	4.76	5.10	4.61	4.56	4.76	4.64
Ho	0.68	0.53	0.50	0.46	0.89	1.04	0.97	0.96	0.92	0.87
Er	1.77	1.35	1.32	1.23	2.30	2.57	2.40	2.44	2.40	2.43
Tm	0.22	0.19	0.16	0.15	0.30	0.32	0.32	0.33	0.33	0.33
Yb	1.40	1.09	1.05	0.88	1.87	2.03	1.95	2.06	2.09	2.00
Lu	0.19	0.13	0.12	0.12	0.27	0.30	0.29	0.30	0.28	0.27
Hf	2.72	2.41	2.19	2.38	5.04	5.83	5.31	5.42	4.41	4.44
Ta	0.97	0.84	0.84	0.95	1.42	1.81	1.63	1.74	1.51	1.50
Pb	2.17	0.85	0.70	0.81	6.24	4.95	5.88	6.66	4.65	4.04

Table 2 continued

Sample	DT1206	DT1413	DT1414	DT1415	11DT01	DT1201	DT1202	DT1203	DT1401	DT1402
Group	Pic	Pic	Pic	Pic	I	I	I	I	I	I
Th	1.91	1.85	1.84	1.91	4.03	3.55	4.13	4.22	3.95	3.96
U	0.50	0.41	0.41	0.48	0.94	1.11	0.89	0.93	0.88	0.93
Sample	DT1403	DT1404	DT1405	DT1406	DT1407	HM1103	HM1104	11DT02	11DT03	DT1204
Group	I	I	I	I	I	II	II	II	II	II
Major elements (wt%)										
SiO_2	48.20	48.30	48.50	48.70	48.80	48.17	47.13	48.36	47.65	47.56
TiO_2	2.27	2.23	2.28	2.04	1.96	1.62	1.18	0.88	1.11	1.04
Al_2O_3	13.55	13.90	13.60	13.45	11.05	14.96	15.40	15.21	16.49	15.62
Fe_2O_3	12.10	11.97	12.20	12.60	12.04	11.41	10.58	10.11	10.68	10.56
MnO	0.18	0.17	0.18	0.18	0.17	0.19	0.16	0.16	0.16	0.18
MgO	6.76	6.39	6.81	7.35	9.59	7.86	8.97	8.29	8.12	9.52
CaO	9.82	9.47	9.81	9.75	10.70	9.11	9.57	12.20	11.30	10.53
Na_2O	2.84	2.58	2.69	2.54	2.29	2.46	2.09	2.10	2.18	2.27
K2O	1.21	1.26	1.26	0.63	0.69	1.29	1.20	0.53	0.43	0.65
P_2O_5	0.25	0.25	0.26	0.21	0.18	0.25	0.16	0.07	0.10	0.12
LOI	1.92	1.93	1.89	1.73	2.09	1.96	2.89	1.43	1.13	1.64
Total	99.10	98.45	99.48	99.18	99.56	99.26	99.31	99.35	99.35	99.69
$Mg^{\#}$	52.5	51.4	52.5	53.6	61.2	57.7	62.7	61.9	60.1	64.1
Trace elements (ppm)										
Sc	37.4	34.4	36.7	37.1	43.7	27.6	27.9	44.6	35.5	34.9
V	312	315	312	334	309	178	192	271	226	240
Cr	107	84	126	296	614	326	517	502	373	881
Co	46.5	45.7	46.8	52.5	54.3	39.6	44.4	42.4	47.8	42.9
Ni	112	95.8	123	142	260	41.0	42.1	21.2	9.78	21.8
Cu	151	124	172	113	176	21.6	25.2	15.8	28.9	22.1
Zn	124	118	124	123	99.9	103	112	65.7	99.5	107
Ga	19.8	20.7	20.2	20.3	17.2	15.6	15.3	14.3	14.8	15.8
Rb	41.0	44.2	37.7	22.0	17.0	83.7	73.4	13.4	11.3	34.2
Sr	520	572	571	503	391	272	280	214	240	240
Y	23.3	23.6	24.3	21.7	20.0	25.8	22.0	16.7	12.6	20.3
Zr	187	200	195	171	157	126	92.4	54.3	36.0	58.2
Nb	26.8	26.8	27.6	15.4	17.8	8.18	5.78	3.74	2.62	2.46
Cs	0.46	0.85	0.74	0.59	0.36	0.69	0.86	0.27	0.26	0.45
Ba	524	395	386	270	304	266	272	157	149	155
La	30.8	31.8	32.4	22.0	24.0	15.3	15.1	7.26	5.73	7.13
Ce	66.9	69.0	69.3	50.7	54.0	31.4	26.0	16.1	12.5	16.8
Pr	7.84	8.10	8.11	6.19	6.37	4.38	3.76	2.27	1.49	2.42
Nd	31.0	32.0	32.5	26.1	26.3	18.6	15.2	10.1	6.80	11.4
Sm	5.81	6.11	6.32	5.52	5.11	4.45	3.67	2.52	1.79	3.12
Eu	1.93	2.04	2.09	1.81	1.67	1.49	1.25	0.98	1.02	1.23
Gd	5.64	5.41	5.81	5.06	4.96	4.41	3.75	2.81	1.99	3.32
Tb	0.89	0.87	0.87	0.82	0.72	0.76	0.66	0.48	0.37	0.62
Dy	4.60	4.46	4.58	4.36	4.07	4.80	4.12	3.16	2.47	3.53
Ho	0.90	0.90	0.92	0.82	0.77	1.02	0.83	0.65	0.51	0.82
Er	2.38	2.40	2.37	2.27	1.89	2.66	2.19	1.70	1.32	2.21
Tm	0.33	0.31	0.32	0.29	0.24	0.38	0.31	0.24	0.17	0.31
Yb	2.01	2.02	2.10	1.78	1.57	2.46	2.09	1.54	1.20	2.00

Table 2 continued

Sample	DT1403	DT1404	DT1405	DT1406	DT1407	HM1103	HM1104	11DT02	11DT03	DT1204
Group	I	I	I	I	I	II	II	II	II	II
Lu	0.29	0.28	0.31	0.25	0.23	0.37	0.30	0.23	0.18	0.31
Hf	4.51	4.56	4.48	4.30	3.96	3.24	2.79	1.60	1.15	1.96
Ta	1.49	1.48	1.59	0.93	1.06	0.47	0.38	0.21	0.18	0.15
Pb	5.07	3.76	5.32	2.81	8.97	3.21	3.84	1.62	1.84	2.63
Th	3.73	4.02	3.92	2.30	3.25	2.59	1.90	0.62	0.55	0.66
U	1.15	0.87	0.80	0.46	0.66	0.64	0.54	0.12	0.26	0.18

Sample	DT1205	11DT04	DT1408	DT1409	DT1410	DT1411	DT1412	DT1416	DT1417
Group	II	II	II	II	II	II	II	II	II
Major elements (wt%)									
SiO_2	52.54	46.64	47.90	46.90	47.20	47.00	46.80	45.40	45.70
TiO_2	0.31	3.60	1.54	3.53	3.58	2.30	2.31	1.73	1.76
Al_2O_3	15.42	12.92	15.35	13.35	13.30	14.85	14.80	16.05	16.15
Fe_2O_3	9.21	16.14	12.22	16.64	16.72	14.92	14.98	11.78	11.63
MnO	0.15	0.27	0.21	0.27	0.28	0.24	0.23	0.21	0.21
MgO	7.06	5.03	7.32	5.14	5.13	6.47	6.59	8.77	8.42
CaO	10.65	8.68	9.68	8.68	8.64	8.81	8.55	7.93	7.81
Na_2O	2.79	2.38	2.26	2.67	2.57	1.86	2.23	2.53	2.61
K2O	0.47	1.37	1.24	0.91	1.02	0.83	0.59	1.40	1.44
P_2O_5	0.02	0.45	0.23	0.47	0.46	0.30	0.30	0.17	0.16
LOI	0.65	1.49	1.57	1.14	1.00	2.34	2.41	4.16	3.99
Total	99.27	98.97	99.52	99.70	99.90	99.92	99.79	100.13	99.88
$Mg^{\#}$	60.3	38.2	54.3	38.0	37.8	46.2	46.6	59.6	58.9
Trace elements (ppm)									
Sc	33.9	48.3	51.4	65.3	58.5	33.9	54.5	50.5	52.0
V	205	249	231	254	237	205	226	240	245
Cr	270	97	360	125	99	256	275	444	402
Co	33.9	44.0	44.2	49.5	40.5	33.9	43.1	53.1	49.7
Ni	13.8	6.97	17.2	13.5	13.3	13.8	42.1	171	128
Cu	13.6	45.4	27.6	39.9	32.0	13.6	36.1	51.6	43.8
Zn	95.9	256	117	187	182	95.9	149	173	169
Ga	17.7	23.5	18.3	24.6	23.9	17.7	21.0	19.3	19.7
Rb	10.3	80.0	97.6	51.3	60.3	10.3	39.7	97.9	99.1
Sr	266	216	262	232	240	266	275	449	447
Y	35.0	57.1	34.9	57.1	57.6	35.0	43.2	33.8	34.8
Zr	108	213	134	228	241	108	154	116	116
Nb	4.41	13.9	7.56	12.9	13.0	4.41	7.46	4.16	3.91
Cs	0.17	0.90	2.73	0.75	0.77	0.17	1.05	1.24	1.19
Ba	114	526	200	361	361	114	207	252	243
La	16.8	28.2	13.5	24.6	25.2	16.8	13.4	9.11	9.15
Ce	34.1	59.4	31.8	56.9	58.4	34.1	31.9	23.1	23.4
Pr	4.46	7.58	3.97	7.42	7.60	4.46	4.26	3.29	3.29
Nd	18.7	34.1	17.9	34.2	34.5	18.7	19.6	16.0	16.4
Sm	4.98	8.72	4.64	8.78	8.66	4.98	5.53	4.59	4.54
Eu	1.18	2.58	1.51	2.85	2.84	1.18	2.01	1.62	1.82
Gd	5.10	9.88	5.26	9.39	9.56	5.10	6.43	5.13	5.23
Tb	1.05	1.73	0.95	1.65	1.67	1.05	1.14	0.93	0.98
Dy	6.19	10.8	6.16	10.0	10.3	6.19	7.32	5.91	5.94

Table 2 continued

Sample	DT1205	11DT04	DT1408	DT1409	DT1410	DT1411	DT1412	DT1416	DT1417
Group	II	II	II	II	II	II	II	II	II
Ho	1.43	2.19	1.25	2.12	2.21	1.43	1.57	1.26	1.34
Er	3.84	5.89	3.56	5.92	6.29	3.84	4.52	3.49	3.74
Tm	0.56	0.84	0.55	0.88	0.80	0.56	0.68	0.50	0.54
Yb	3.66	5.26	3.29	5.51	5.54	3.66	4.09	3.21	3.29
Lu	0.54	0.79	0.51	0.80	0.83	0.54	0.60	0.49	0.51
Hf	3.46	6.40	3.21	5.60	6.03	3.46	4.10	3.07	2.93
Ta	0.35	0.66	0.37	0.70	0.72	0.35	0.41	0.23	0.20
Pb	3.05	9.85	3.58	6.80	5.70	3.05	2.25	2.01	1.88
Th	1.35	1.92	0.84	1.82	1.88	1.35	0.89	0.68	0.65
U	0.49	0.49	0.65	0.75	0.46	0.49	0.16	0.14	0.12

$Mg^{\#} = 100 \times (MgO/(MgO + FeO_T))$, molar; assuming $FeO_T = 0.9 \times Fe_2O_3$

Pic picritic rocks, *LOI* loss on ignition

rocks exhibit moderately LREE-enriched and HREE-depleted patterns in the chondrite-normalized REE diagram (Fig. 5c), and have La_N values of 18–91, $(La/Yb)_N$ ratios of 1.9–4.9, $(La/Sm)_N$ ratios of 1.3–2.6 and $(Gd/Yb)_N$ ratios of 1.1–1.5. Overall, the contents of total REE (REE = 37.6–178 ppm) and other incompatible trace elements in the Group II mafic rocks are lower than those of Group I mafic rocks (Fig. 5). Some samples of the Group II mafic rocks display obviously positive Eu anomalies (e.g., 11DT03 with $\delta Eu = 1.6$), but some others display negative Eu anomalies (e.g., DT1205 with $\delta Eu = 0.71$) (Fig. 5c), which is different from the Group I mafic rocks with insignificant Eu anomalies ($\delta Eu = 0.96–1.1$; Fig. 5a). In the primitive mantle-normalized spider diagram (Fig. 5b, d), the Group I mafic dykes show "humped" patterns that are similar to the picritic dyke, whereas the Group II mafic rocks are moderately enriched in LILE and depleted in HFSE. Many samples from the Group II mafic dykes still show variable Ti anomalies relative to the neighboring elements. In addition, the Group I mafic rocks only display slightly negative to insignificant Nb–Ta anomalies [$(Nb/La)_P = 0.67–0.95$], but the Group II mafic rocks are obviously depleted in Nb and Ta relative to La [$(Nb/La)_P = 0.25–0.54$] (Fig. 5b, d).

On the Nb/Y versus Zr/TiO_2 plot of Winchester and Floyd (1976), the Group I mafic and the picritic rocks plot as a fairly tight cluster within the alkaline basalt field, whereas the Group II mafic rocks are plot in the sub-alkaline basalt field (Fig. 6a) and mainly show the tholeiitic basaltic affinities (Fig. 6b). In addition, Ti/Y ratios, rather than TiO_2, are used as a discriminator of rock types, because TiO_2 contents generally increase but Ti/Y ratios does not vary much during fractional crystallization (Peate et al. 1992). On the Ti/Y versus Nb/Y plot of Peate et al. (1992), the Group I mafic and the picritic rocks are characterized by high Ti/Y ratios (576–946) similar to the high Ti basaltic rocks, but the Group II mafic rocks have low Ti/Y ratios (<500) which is similar to the low-Ti basaltic rocks (Fig. 6c).

Nd isotopes

Samarium–Neodymium isotopic data for the Datian mafic–ultramafic dykes in the Panzhihua area are given in Table 3. The picritic samples have $^{147}Sm/^{144}Nd$ values of 0.1223–0.1334, $^{143}Nd/^{144}Nd$ ratios of 0.512476–0.512492, corresponding to $\varepsilon_{Nd}(T)$ values of +3.0 to +4.4. The Sm–Nd isotopic compositions of the Group I mafic samples are similar to that of the picritic samples, but different from that of the Group II mafic rocks. The Group I mafic and Group II mafic samples have $^{147}Sm/^{144}Nd$ values of 0.1218–0.1316 and 0.1445–0.1816, $^{143}Nd/^{144}Nd$ ratios of 0.512483–0.512580 and 0.512253–0.512546, corresponding to $\varepsilon_{Nd}(T)$ values of +4.3 to +5.2 and −3.3 to +1.1, respectively.

Discussion

Fractional crystallization and crustal contamination

As basaltic magmas erupted within continental settings are likely to have undergone variable degrees of fractional crystallization and crustal contamination, which may affect the magma composition, it is necessary to evaluate the possible fractional crystallization and crustal contamination processes before attempting to use geochemical signatures of these rocks to constrain the potential mantle source.

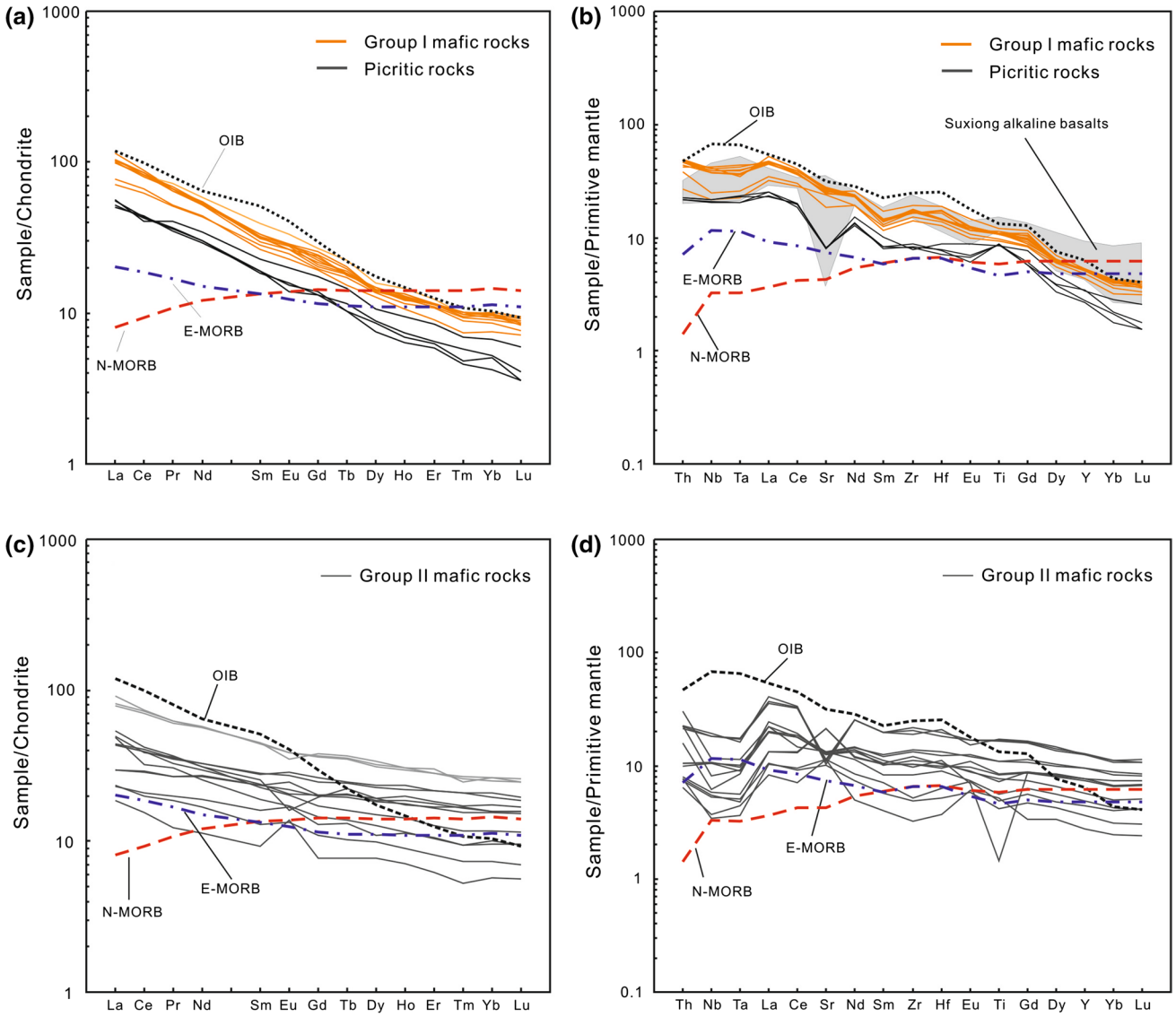

Fig. 5 Chondrite-normalized REE patterns (**a**, **c**) and primitive mantle-normalized incompatible trace element spidergram (**b**, **d**) for the Datian mafic–ultramafic dykes. The normalizing values for chondrite are from Boynton (1984). The normalizing values of the primitive mantle are from Sun and McDonough (1989). The compositions of OIB, E-MORB and N-MORB for comparison are also from Sun and McDonough (1989). The values of the Suxiong alkaline basalts are from Li et al. (2002a)

Fractional crystallization

Mantle-derived primary magma generally have Ni > 400 ppm, Cr > 1000 ppm (Wilson 1989) and $Mg^{\#}$ = 73–81 (Sharma 1997 and references therein). The high $Mg^{\#}$ (75.7–76.3), Cr (1957–2260 ppm) and Ni contents (726–1465 ppm) of the picritic dyke indicate the composition is close to the mantle-derived primary magma. Both the Groups I and II mafic dykes, however, have low $Mg^{\#}$, Ni and Cr content (Table 2), suggesting that they may have undergone significant fractionation of olivine, spinel and/or clinopyroxene during magma evolution. Near-positive correlations between CaO and MgO contents of the Group II mafic rocks imply the likely fractional crystallization of clinopyroxene (Fig. 7). For the Group I mafic rocks, significant fractional crystallization of plagioclase did not occur because of the absence of Eu anomaly (Fig. 5a, b). However, some samples (e.g., 11DT03 and DT1205) from the Group II mafic rocks display obvious Eu anomalies in the chondrite-normalized REE patterns (Fig. 5c), suggesting that they may undergo some plagioclase fractionation or accumulation. The TiO_2, $Fe_2O_3^T$ and P_2O_5 contents of the Groups I and II mafic rocks increase or keep constant with decreasing MgO contents (Fig. 7), suggesting insignificant role of Fe–Ti oxide and apatite during fractional crystallization.

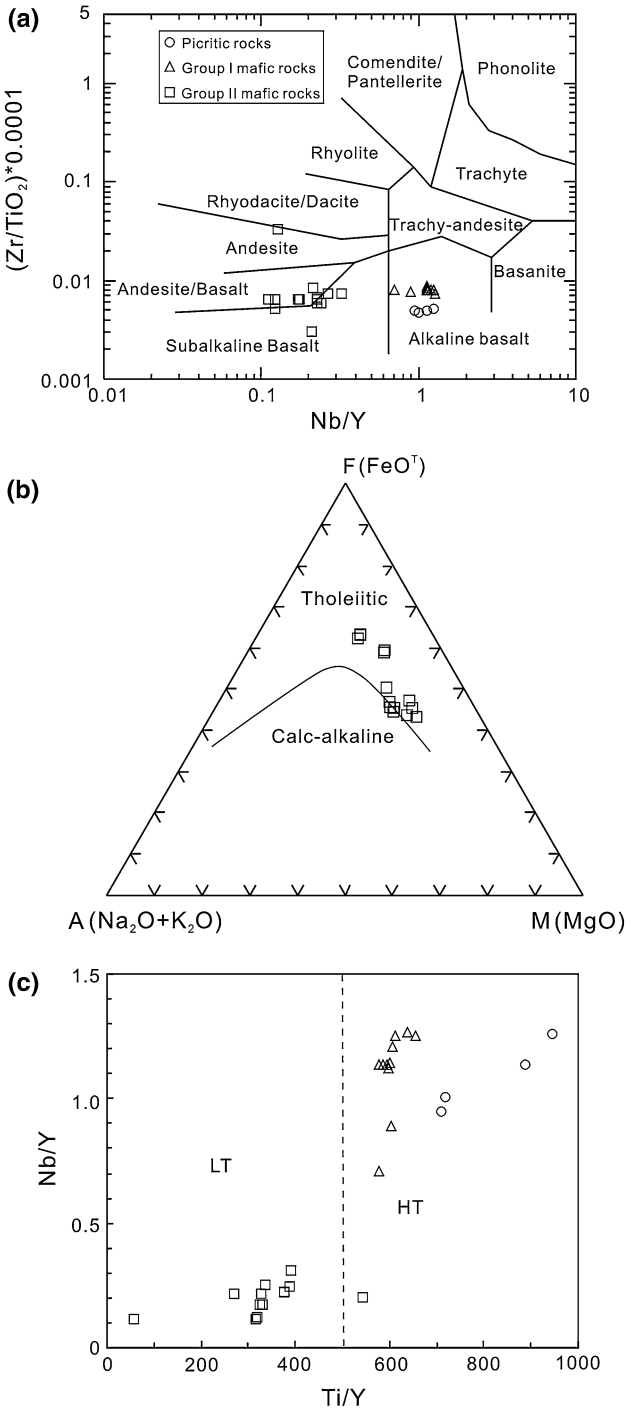

Fig. 6 Plots of **a** Nb/Y versus Zr/TiO_2 (Winchester and Floyd 1976), **b** whole-rock alkali ($Na_2O + K_2O$)–FeO^T–MgO (AFM), and **c** Ti/Y versus Nb/Y (Peate et al. 1992) of the Datian mafic–ultramafic dykes

The mantle olivine have forsterite (Fo) content of 91 (e.g., Albaredè 1992), and thus the mantle-derived primary melt that is in equilibrium with the mantle olivine should have Fe/Mg (mole) ratios of 0.33, assuming K_D $(FeO/MgO)^{olivine}/(FeO/MgO)^{liquid}$ of 0.3 between olivine and basaltic magma (Roeder and Emslie 1970). The picritic rocks have Fe/Mg ratios of 0.31–0.32, also indicating the compositions of picritic rocks are close to that of primary magma. The Group I mafic and picritic rocks exhibit near-parallel chondrite-normalized REE patterns and similar primitive mantle-normalized incompatible element patterns (Fig. 5a, b). In addition, the Group I mafic rocks and the picritic rocks have similar Nd isotopic compositions, implying that they were likely cogenetic. The Group I mafic rocks have higher incompatible trace element contents than those of the picritic rocks (Fig. 5a, b). These together with lower Ni, Cr contents and $Mg^{\#}$ values of the Group I mafic dykes (Table 2) indicates it may evolve from the magma parental to the picritic dyke by fractionation of olivine, spinel and/or clinopyroxene, or different degrees partial melting of the mantle source.

The evolution paths from the picritic magma to the basaltic magma were simulated using the MELTS package (Ghiorso and Sack 1995), at fO_2 of FMQ (fayalite–magnetite–quartz) and pressure of 2 kbar under hydrous conditions (H_2O = 1 wt%). The least differentiated sample DT1415 [lowest $Mg^{\#}$, and highest $\varepsilon_{Nd}(T)$ value of +4.4 and Fe/Mg ratios of 0.32; Tables 2 and 3] of the picritic rocks was used as the primary composition of the mantle-derived magma. The MELTS calculation indicates that at 2 kbar, olivine is the first phase to appear on the liquids (1485 °C), followed by spinel and pyroxenes (Fig. 8). When the temperature decreases to ~1135 °C after fractional crystallization of ~39.3 % olivine, ~2.03 % spinel and ~14.7 % clinopyroxene, the major oxide contents in the residual liquid is comparable to the average composition of the Group I dolerite rocks (Table 4). Although it deserves further assessment, it can be considered that the Group I dolerite rocks may evolve from the magma parental to the picritic dyke by fractionation of olivine, spinel and clinopyroxene.

Crustal contamination

The picritic dyke and the Group I mafic dykes are characterized by a very slight depletion in Nb–Ta relative to the neighboring elements in the primitive mantle-normalized spider diagram (Fig. 5b) and relatively homogeneous Nd isotopic compositions, suggesting negligible crustal contamination involved in the magma. In contrast, the Group II mafic rocks show distinctly negative Nb–Ta anomalies relative to the neighboring elements [$(Nb/La)_P$ = 0.25–0.54] and variable Nd isotopic compositions [$\varepsilon_{Nd}(T)$ = −3.3 to +1.1; Table 3]. In general, the addition of crustal material to basaltic magmas during magma evolution is expected to produce a positive covariance of $\varepsilon_{Nd}(T)$ values with MgO (Fig. 9a), a negative covariance of $\varepsilon_{Nd}(T)$ values with SiO_2 (Fig. 9b) and incompatible trace element ratios such as La/Sm (Fig. 9c; Taylor and McLennan 1995). It is therefore

Table 3 Sm–Nd isotopic compositions for the Datian mafic–ultramafic dykes in the Panzhihua area, SW China

Sample	Group	Sm (ppm)	Nd (ppm)	$^{147}Sm/^{144}Nd$	$^{143}Nd/^{144}Nd$	2σ	$(^{143}Nd/^{144}Nd)_I$	$\varepsilon_{Nd}(T)$	Method
DT1206	Pic	4.240	19.23	0.1334	0.512476	0.000002	0.511812	3.0	TIMS
DT1415	Pic	3.706	18.34	0.1223	0.512492	0.000002	0.511884	4.4	TIMS
DT1202	I	6.530	32.44	0.1218	0.512509	0.000004	0.511902	4.8	TIMS
DT1402	I	6.316	31.37	0.1218	0.512483	0.000004	0.511877	4.3	TIMS
DT1406	I	5.528	25.42	0.1316	0.512580	0.000002	0.511926	5.2	TIMS
HM1103	II	4.45	18.6		0.512253	0.000013	0.511495	−2.2	MC–ICP–MS
DT1409	II	8.78	34.2		0.512364	0.000005	0.511550	−1.1	MC–ICP–MS
DT1412	II	5.53	19.6		0.512427	0.000013	0.511532	−1.4	MC–ICP–MS
11DT04	II	8.72	34.1		0.512356	0.000005	0.511545	−1.2	MC–ICP–MS
DT1408	II	4.64	17.9		0.512307	0.000006	0.511485	−2.4	MC–ICP–MS
11DT02	II	2.506	9.59	0.1581	0.512264	0.000010	0.511438	−3.3	TIMS
DT1204	II	2.959	10.93	0.1637	0.512523	0.000010	0.511664	1.1	TIMS
DT1417	II	5.292	17.63	0.1816	0.512546	0.000004	0.511595	−0.20	TIMS

Chondrite uniform reservoir (CHUR) values ($^{147}Sm/^{144}Nd = 0.1967$, $^{143}Nd/^{144}Nd = 0.512638$) are used for the calculation. $\lambda_{Sm} = 6.54 \times 10^{-12}$ year^{-1} (Lugmair and Harti 1978). The $(^{143}Nd/^{144}Nd)_I$ and $\varepsilon_{Nd}(T)$ of the picritic rocks and the Group I mafic rocks from the Datian area were calculated using the age of 760 Ma. The Group II mafic rocks were calculated using the age of 800 Ma

suggested that the magmas parental to the Group II mafic rocks probably experienced some degrees of crustal assimilation during fractional crystallization.

Mantle source characteristics and degrees of partial melting

The picritic dyke and the Group I mafic dykes

The picritic dyke and the Group I mafic dykes display OIB-like trace elements patterns and REE patterns with very slight Nb–Ta negative anomalies due to slightly crustal contamination (Fig. 5a, b). In addition, most samples of the picritic dyke and the Group I mafic rocks show similar trace element patterns with the Suxiong alkaline basalts (~803 Ma) in the western margin of the Yangtze Block (Li et al. 2002a) (Fig. 5b), implying that the magma parental to these rocks was generated by melting of OIB and CFB-like mantle source (Fig. 5c, d). Obviously positive $\varepsilon_{Nd}(T)$ values (+3.0 to +5.2) (Table 3) suggest that the picritic and the Group I mafic dykes were originated from a time-integrated depleted mantle source. During partial melting, the residual mineralogy of the magma source is one of the most important factors influencing the compositions of basaltic magmas. The steep REE patterns and high Sm/Yb ratios of the picritic rocks and the Group I mafic rocks are indicative of small melt fractions and/or garnet control (Fig. 5a; van Westrenen et al. 2000; Adam and Green 2006). As shown in a plot of Sm/Yb versus Sm (Fig. 10a), the picritic rocks are most likely derived from a garnet control mantle source, because the small degree partial melting of spinel-bearing mantle source could not produce such a picritic magma in this study. Moreover, garnet has a high partition coefficient for Y ($D_{garnet/melt} = 3.1$) relative to Ti ($D_{garnet/melt} = 0.29$) (Johnson 1998). The high Ti/Y ratios (Fig. 6c) of these rocks further indicate a mantle source at a garnet stable field.

The degree of partial melting of the mantle source for the picritic and the Group I mafic rocks was modeled by REE abundances and ratios using the non-modal batch melting standard equations of Shaw (1970), in which the REE partition coefficients are from McKenzie and O'Nions (1991). As shown in Fig. 10b, in order to produce the La/Sm ratios and La contents of the picritic rocks, a mantle source with the composition of depleted mantle (DM; Salter and Stracke 2004) and the primitive mantle (PM; Sun and McDonough 1989) has to melt in degrees of less than 1 % and ca. 3 %, respectively. Such circumstances cannot meet the major oxides for these picritic rocks. As a result, their mantle sources should be more enriched in incompatible trace elements than primitive mantle but still depleted in Nd isotopic composition. Extrapolation of the likely partial melting trajectories drawn for the Datian picritic rocks gives 25 % of partial melting of a mantle source (shown as G1 on the mantle array; Fig. 10b). Furthermore, the relatively high platinum group element (PGE) contents (19.7–29.0 ppb; Yang et al. 2016) of the Group I-Pic ultramafic rocks means no sulfide segregation, implying that there were no residual sulfides in the mantle source. To dissolve all sulfides in the mantle-derived magma, ca. 18 % (Naldrett 2010) or ca. 25 % (Keays 1995) of partial melting in the mantle is required.

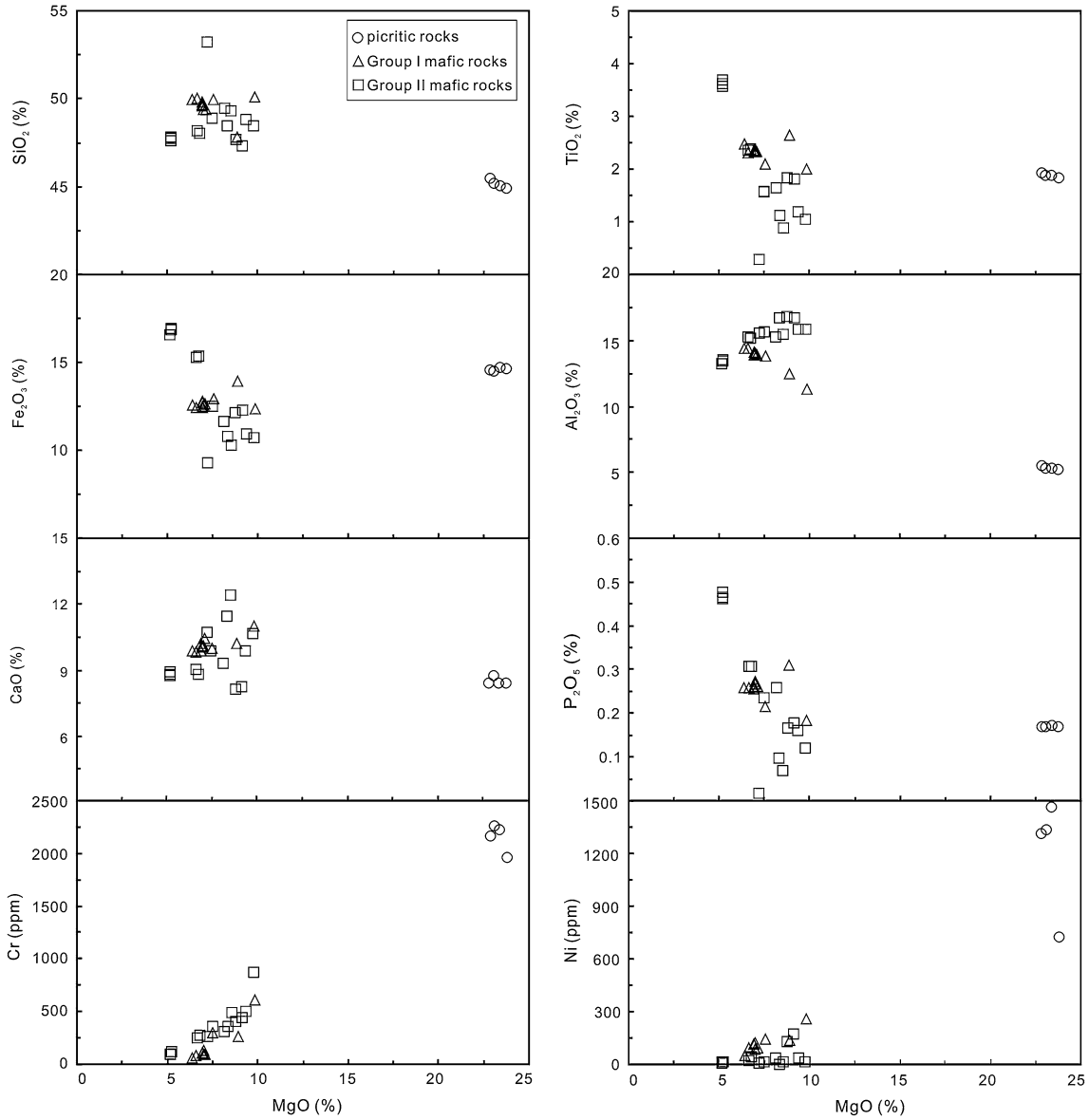

Fig. 7 Fenner diagrams for the Datian mafic–ultramafic dykes

The Group II mafic dykes

Compared with the picritic rocks and the Group I mafic rocks, most of the Group II mafic rocks exhibit obviously lower $\varepsilon_{Nd}(T)$ values (+1.1 to −3.3; Table 3) and ∑REE contents and LREE/HREE ratios (Table 2; Fig. 5). Moreover, the Group II mafic rocks show tholeiitic basaltic affinities rather than alkaline basaltic affinities (Fig. 5a, b). In addition, the forming age of the Group II mafic rocks are ca. 40 Ma older than that of the picritic rocks and the Group I mafic rocks. All these above suggest the Group II mafic rocks have different mantle source with that of picritic rocks and the Group I mafic rocks.

The Group II mafic rocks have relatively lower La/Yb ratios (2.78–7.20) than that of the picritic and the Group I mafic rocks, which reflect a melting regime dominated by relatively large melt fractions and/or spinel as the predominant residual phase. Relatively low Ti/Y ratios of the Group II mafic rocks (Fig. 6c) suggest the absence of garnet in the mantle source. Melting of a spinel peridotite will result in a minimal variation in MREE/HREE ratios (e.g., Sm/Yb) with melt fraction because *D*Cpx Sm is nearly equal to *D*Cpx Yb (McKenzie and O'Nions 1991), even in near sub-solidus clinopyroxene (Blundy et al. 1998). The low Sm/Yb ratios of the Group I rocks further imply spinel is the predominant residual phase (Fig. 10a).

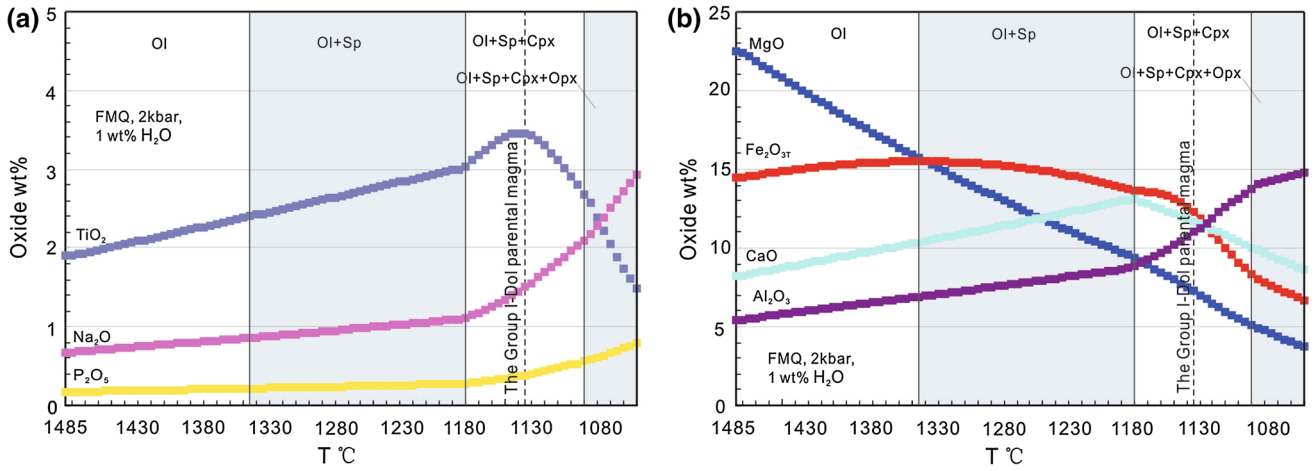

Fig. 8 MELTS modeling of fractionation of magma in the magma chamber under FMQ, 2 kbar and 1 wt% H_2O. *Ol* olivine, *Sp* spinel, *Cpx* clinopyroxene, *Opx* orthopyroxene

Table 4 Comparison between the compositions of the residual liquid calculated using MELTS and the average compositions of Group I mafic rocks (oxides in wt%)

	SiO_2	TiO_2	Al_2O_3	$Fe_2O_3^T$	MnO	MgO	CaO	Na_2O	K_2O	P_2O_5	Cr_2O_3	NiO	H_2O
PM	44.79	1.90	5.47	14.33	0.18	22.50	8.27	0.68	0.22	0.17	0.33	0.18	1.00
RL	49.37	3.45	11.00	12.28	0.18	7.25	11.71	1.50	0.50	0.38	0.07	0.04	2.26
AC	49.58	2.33	13.68	12.71	0.18	7.38	10.15	2.66	1.07	0.25	0.03	0.01	

PM represents the primary magma of the picritic rocks, taking the sample DT1415 as it is approximation; RL represents the residual liquid, when the temperature decreases to ~1135 °C after fractional crystallization of ~39.3 % olivine, ~2.03 % spinel and ~14.7 % clinopyroxene; AC represents the average composition of Group I mafic rocks

The correlations as shown in Fig. 9 suggest that the magmas parental to the Group II mafic rocks have experienced an assimilation and fractional crystallization process (AFC). In fact, the Nd isotopic composition of the asthenospheric mantle during ca. 800 Ma are very depleted [$\varepsilon_{Nd}(T)$ values of +5.0 to +6.0; Li et al. 2002a]. Thus, the magmas parental to the Group II mafic rocks may not only be formed by crustal contamination of the magma derived from asthenospheric mantle, as a high-proportional input of crustal materials is needed which seems impossible. Moreover, the depletion of Nb and Ta should be more prominent with the increasing degrees of assimilation. The Group II mafic rocks show no such features, implying their Nb–Ta depletions are not only controlled by crustal contamination, but also originated from their mantle source. A spinel-bearing mantle source also implies a shallow melting zone (<80 km; Takahashi and Kushiro 1983) and is likely located in the sub-continental lithosphere mantle (SCLM). SCLM can preserve distinct geochemical signatures such as those induced by infiltration of asthenospheric melts resulted from a rising mantle plume or of fluid and melts derived from subduction (Sprung et al. 2007 and references therein). There is a secular evolution from depleted Archean SCLM to more fertile Phanerozoic SCLM (Griffin et al. 2009; Tang et al. 2013), and thus, the SCLM beneath the Yangtze Block should display the characteristic of relative enrichment during Proterozoic. This feature is consistent with the Nd isotopic composition of the Group II mafic rocks [$\varepsilon_{Nd}(T)$ values: +1.1 to −3.3]. Therefore, different from the picritic and the Group I mafic dykes, the Group II mafic dykes may derive from SCLM.

Tectonic significance in relation to the supercontinent Rodinia

In the western margin of the Yangtze Block, there are numerous Neoproterozoic magmatic rocks, mainly including mafic–ultramafic and felsic magmatic rocks. These rocks can be generally grouped into two major populations according to their ages: ca. 830–795 and 780–740 Ma. For their origination, two major models are proposed: plume-rift model and collision-arc model. (1) Plume-rift model: the ca. 830–745 Ma magmatic rocks in the South China are the results of a mantle superplume beneath supercontinent

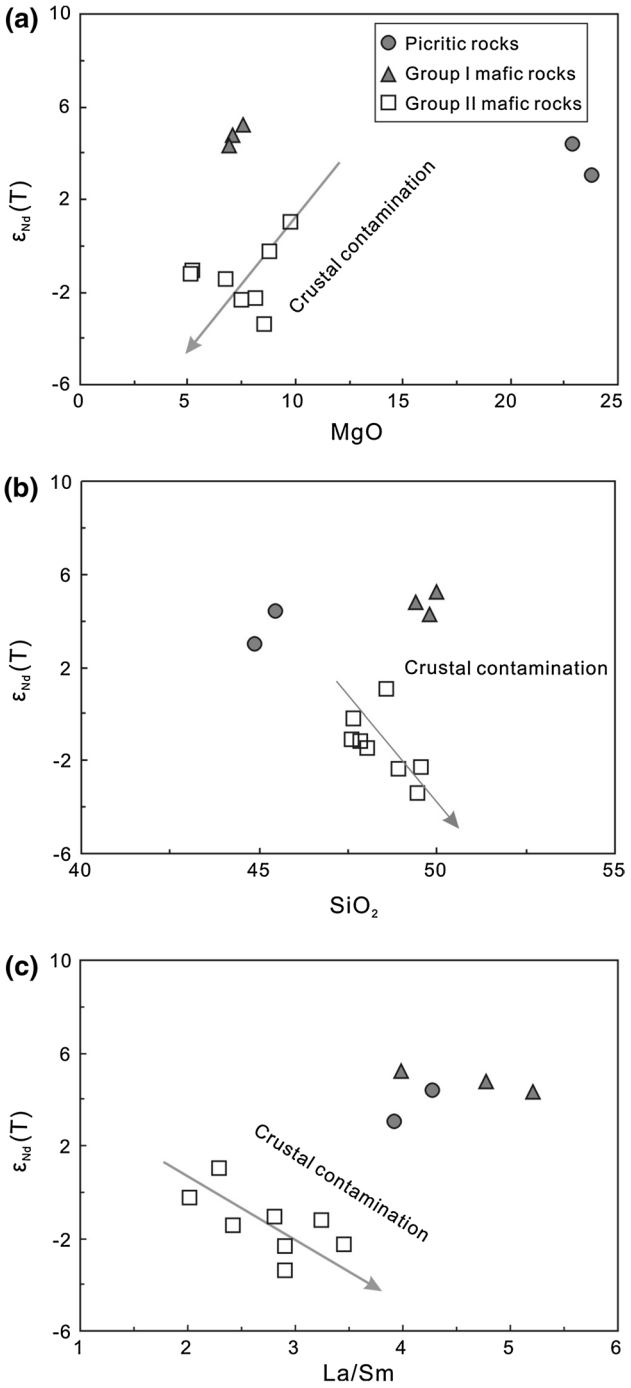

Fig. 9 Plots of **a** $\varepsilon_{Nd}(T)$ versus MgO, **b** $\varepsilon_{Nd}(T)$ versus SiO_2, and **c** $\varepsilon_{Nd}(T)$ versus La/Sm for the Datian mafic–ultramafic dykes

Rodinia, and this mantle superplume was responsible for the breakup of the supercontinent during Neoproterozoic time. The ca. 830–795 Ma is the first phase, started prior to the continental rifting and peaked at the beginning of the rifting at ca. 820 Ma, whereas the ca. 780–740 Ma, as the second phase, occurred during the continental rifting (e.g., Li et al. 1999, 2002a, 2003a, b, 2006). (2) Collision-arc model: the ca. 860–740 Ma magmatic rocks in the western margin of the Yangtze Block are arc-related, caused by the subduction of oceanic lithosphere eastward (present-day orientation) underneath the Yangtze Block during Neoproterozoic time (e.g., Zhou et al. 2002a, b, 2006; Zhao and Zhou 2007a, b). The new data of this study for the ca. 800 Ma and ca. 760 Ma Datian mafic–ultramafic dykes in the Panzhihua area place new constraints on the Neoproterozoic tectonic evolution on the western margin of the Yangtze Block.

The Ti/V ratio is useful for diagnosing tectonic setting of basaltic rocks, as it is a function of the oxygen fugacity of the magmas and their sources, and the degree of partial melting and fractional crystallization (Shervais 1982). MORB and within-plate basalts have Ti/V ratios ranging from 20 to >50, while island-arc basalts typically have Ti/V < 20 (Vermeesch 2006). The picritic rocks, the Group I mafic and Group II mafic dykes have Ti/V ratios of ca. 45, 38–67 and 9.2–92 (50 in average), respectively, significantly higher than that of arc basalts and in line with values for intraplate basalts. Moreover, as the slope of the Alz–TiO_2 data array of clinopyroxene is also useful for discriminating the tectonomagmatic affiliation of the igneous rock suite (Loucks 1990), a plot of the clinopyroxene data for all the Datian mafic–ultramafic rocks on an Alz–TiO_2 diagram (Fig. 11a) displays that these rocks have a relatively flat slope compared with those formed in arc tectonic settings, indicating a rift-origin for these mafic–ultramafic rocks. In addition, the picritic rocks and the Group I mafic rocks exclusively plot in the field of intra-plate setting in the diagram of Zr − Ti/100 − Y × 3 (Fig. 11b). It is notable that in Fig. 11b, most rocks from the Group II mafic dykes are plotted in the island-arc basalt + MORB + calk–alkali basalt field. The Group II mafic dykes experienced obvious crustal contamination and were derived from a SCLM source, and thus, the Fig. 11b is unfit for the Group II rocks to discriminate its tectonic setting. Collectively, the Datian mafic–ultramafic dykes in the area were formed in a within-plate rift environment, rather than an arc environment.

The forming age of the Group II mafic rocks is ~800 Ma, which are broadly concurrent with the ca. 820–810 Ma Tiechuanshan–Bikou CFB (Ling et al. 2003; Wang et al. 2008), the ca. 800 Ma Suxiong bimodal volcanic rocks (Li et al. 2002a) and the ca. 792 Ma Yanbian OIB-like alkaline mafic dykes (Zhu et al. 2008), indicating that significant syn-rift magmatism occurred during 820–790 Ma along the western margin of the Yangtze Block. The ca. 820–790 Ma plume activities beneath South China may trigger the melting of the SCLM source for the Group II mafic dykes in the Panzhihua area. In addition, it is probable that this plume provided enriched components to the source region of the picritic rocks and the Group I mafic rocks. As mentioned in "The picritic dyke and the Group I mafic dykes" section, the mantle source of the picritic rocks and the Group

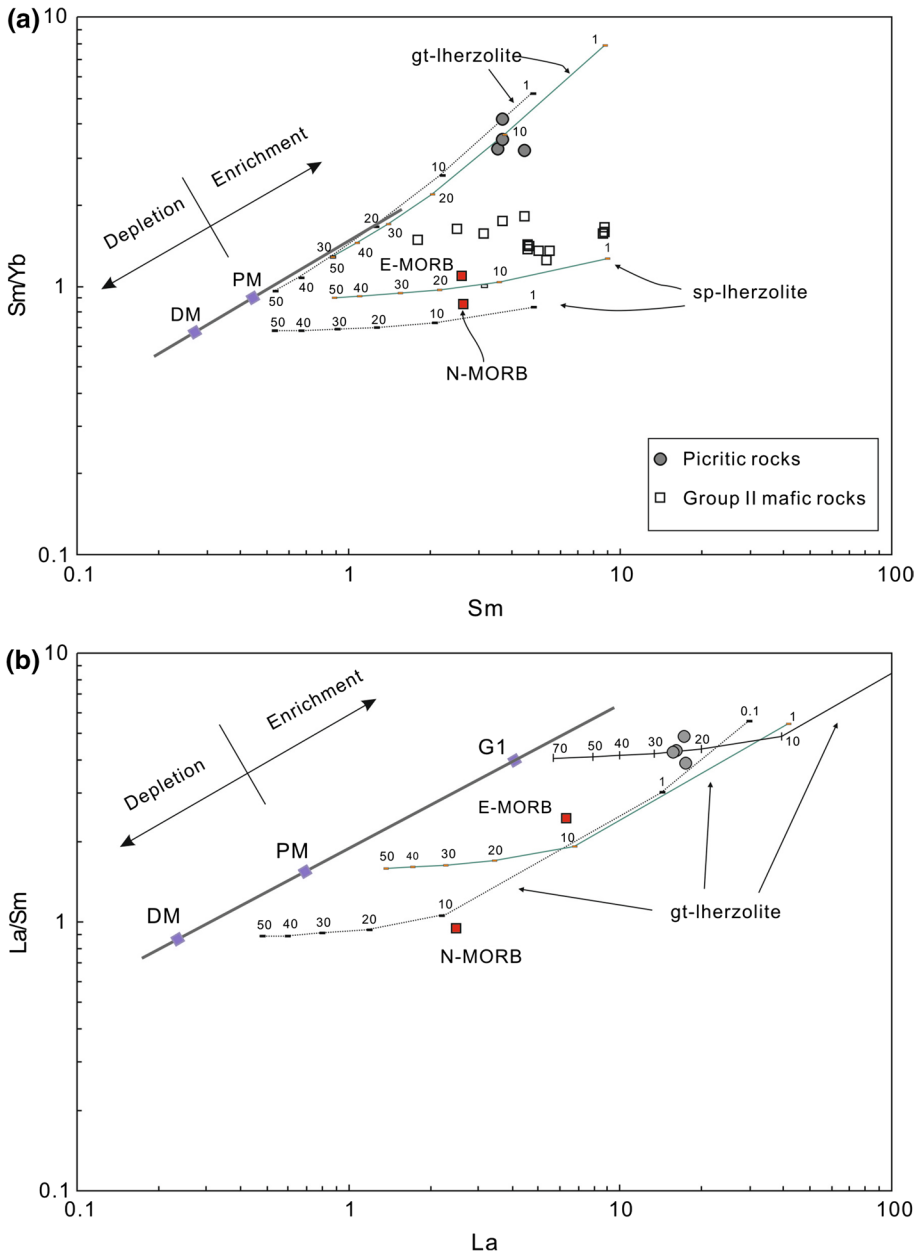

Fig. 10 Plots of Sm/Yb versus Sm (**a**) and La/Sm versus La (**b**) for the Datian mafic–ultramafic dykes. The data of melt curves are obtained using the non-modal batch melting equations of Shaw (1970). Melt curves are drawn for spinel–lherzolite (with mode and melt mode of $ol_{0.530} + opx_{0.270} + cpx_{0.170} + sp_{0.030}$ and $ol_{0.060} + opx_{0.280} + cpx_{0.670} + sp_{0.110}$, respectively; Kinzler 1997) and for garnet–lherzolite (with mode and melt mode of $ol_{0.600} + opx_{0.200} + cpx_{0.100} + gt_{0.100}$ and $ol_{0.030} + opx_{0.160} + cpx_{0.880} + gt_{0.090}$, respectively; Walter 1998). Partition coefficients are from the compilation of McKenzie and O'Nions (1991). DM compositions are from Salter and Stracke (2004). PM, N-MORB and E-MORB compositions are from Sun and McDonough (1989). *G1* represents the mantle source composition of the picritic rocks and the Group I mafic rocks defined by extrapolating the likely melting trajectories drawn for the picritic rocks. The *gray heavy line* represents the mantle array defined using DM and PM compositions

I mafic rocks are enriched in incompatible elements and depleted in Nd isotopic compositions. Many oceanic and continental intraplate alkaline suites that show OIB-like enriched nature with respect to N-type MORB have been attributed to a plume component (e.g., originating below the convectively stirred upper mantle) in the source region (e.g., Hofmann and White 1982; Wilson 1993).

The ca. 760 Ma Group I mafic rocks and picritic rocks are also broadly concurrent with basaltic rocks related to intraplate setting, such as the ca. 780–760 Ma mafic dykes in the Shimian and Kangding areas (Li et al. 2003b; Lin et al. 2007) and the ca. 752 Ma Shaba gabbro (Li et al. 2003b), suggesting significant continental rifting event during 780–740 Ma along the western margin of the Yangtze Block. With the development of continental rift going on, the basaltic magmas usually change from alkaline to tholeiitic in compositions (e.g., Giret and Lameyre 1985). However, the tendency in this study is just the opposite (from tholeiitic to alkaline). Thus, the rifting event generating the Group II mafic dykes might have different genesis to the later rifting that caused the picritic dyke and the Group I mafic dykes. One possible explanation is that multistage rifting events existed during 820–740 Ma in the western margin of the Yangtze Block.

The results of this study provide further evidence for the two phases of rift-related magmatism at ca. 820–790 and 780–740 Ma in the western margin of the Yangtze Block, and

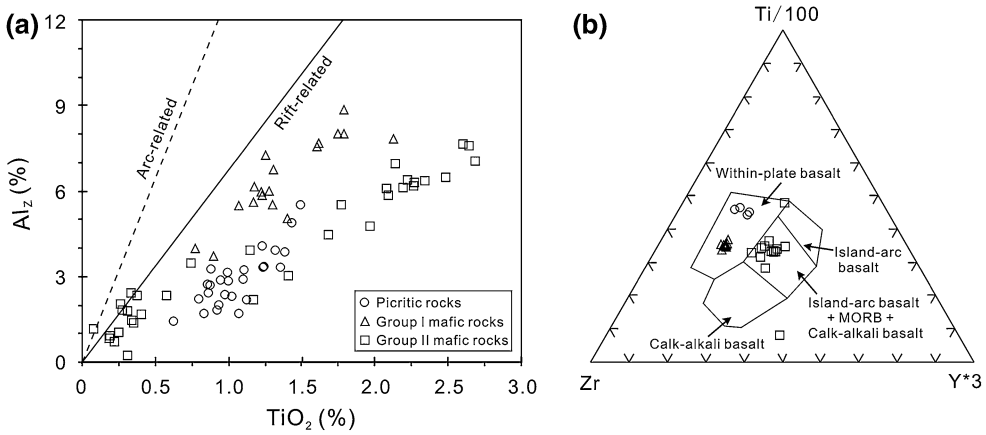

Fig. 11 Discrimination diagrams of **a** Al_Z (percentage of tetrahedral sites occupied by Al) versus TiO_2 in clinopyroxenes (Loucks 1990), **b** Ti–Zr–Y (Pearce and Cann 1973) for the Datian mafic–ultramafic dykes

they are coinciding with the extensive mid-Neoproterozoic mafic–ultramafic magmatism in many continental fragments of supercontinent Rodinia (see detailed discussions in Li et al. 2003b, 2008). In the Panzhihua area, the Dadukou mafic plutons (ca. 740 Ma) and Datian quartz diorite plutons (ca. 760 Ma) were both considered as the products of arc volcanism by some researchers (Zhao and Zhou 2007a, b). Based on this study, they most likely formed within continental rift setting similar to the coeval mafic–ultramafic dykes in the area, and their arc affinities may have originated from SCLM that metasomatized by older subducted-related material.

Collectively, the mafic–ultramafic dykes in the Panzhihua area show mainly alkaline and tholeiitic features. The above discussions suggest that they were formed in a rift setting rather than the products of magmatism of convergent plate boundary. The Neoproterozoic evolution in the area supports a plume-rift model, in which an ascending superplume centered beneath South China at ca. 820 Ma triggered the multistage rifting events in the western margin of the Yangtze Block. This superplume may result in the final breakup of the supercontinent Rodinia, separating South China from southeastern Australia.

Conclusions

The following conclusions are drawn on the basis of this study:

1. SIMS U–Pb zircon and baddeleyite dating results indicate that the Group I mafic dykes and the picritic dyke in the Panzhihua area were emplaced at ~760 Ma, while the Group II mafic dykes were emplaced at ~800 Ma.
2. The picritic rocks and the Group I mafic rocks show "humped" trace element patterns with slightly negative to insignificant Nb–Ta anomalies, and high $\varepsilon_{Nd}(T)$ values of +3.0 to +5.2. The slightly negative to insignificant Nb–Ta anomalies may attribute to minor crustal contamination. The Group II mafic rocks are characterized by a relatively large ranges of $\varepsilon_{Nd}(T)$ values (+1.1 to −3.3) and moderately enrichment of LILE and LREE and depletion in HFSE and HREE, with distinctive negative Nb–Ta anomalies, which could be caused by crustal assimilation and originated from mantle source.
3. The primary magmas of the Group I mafic rocks and the picritic rocks were both derived from the partial melting of an OIB-like, Nd isotopically depleted but incompatible elements relatively enriched mantle source (compare to DM and PM) in a garnet stable field. Modeling results indicate that ca. 25 % batch melting is needed to produce their primary magma. The Group II mafic dykes crystallized from crustal contaminated mafic magmas derived from a spinel-bearing subcontinental lithospheric mantle source.
4. This study suggests that the picritic dyke and the dolerite dykes were both formed in a continental rift setting. In combination with other Neoproterozoic igneous rocks in the western margin of the Yangtze Block, the results support the argument that multistage continental rifting events existed in the area in response to an ascending superplume, which centered beneath South China at ca. 820 Ma.

Acknowledgments We thank X.X. Ling, G.Q. Tang, Q.L. Li and H.X. Ma for the assistances during SIMS dating, B. Wang for major element analyses by XRF, J. Hu and Y. Huang for trace element analyses by ICP–MS, F. Xiao and X.B. Li for Nd isotope analyses by Triton, and J. Wang for Nd isotope analyses by Nu Plasma. The paper benefited from review comments from the editor and two anonymous reviewers. This work was supported by the NSFC (Grants 41273049, 41572074 and 40673031) and the State Key Laboratory of Ore Deposit Geochemistry (12th Five-Year Plan: SKLOG-ZY125-06).

Appendix

See Table 5.

Table 5 Clinopyroxene compositions for the mafic–ultramafic dykes in the Datian area

Sample	DT1206	DT1206	DT1206	DT1206	DT1206	DT1206	DT1206	DT1206	DT1206	DT1413	DT1413	DT1413	DT1413	DT1413	DT1413
Group	Pic	Pic	Pic	Pic	Pic	Pic	Pic	Pic	Pic	Pic	Pic	Pic	Pic	Pic	Pic
SiO_2	53.05	53.00	53.09	53.30	51.78	52.77	52.06	53.94	53.12	53.06	53.28	53.15	53.26	53.08	52.61
TiO_2	0.86	1.11	1.06	0.93	1.22	1.33	1.38	0.63	0.88	0.95	0.80	1.02	1.11	0.86	1.11
Al_2O_3	1.59	2.52	1.77	1.83	2.28	2.83	2.56	1.05	1.61	1.84	1.73	1.84	2.03	1.72	1.89
Cr_2O_3	0.81	0.78	0.61	0.54	0.44	0.87	0.98	0.62	0.72	0.87	1.20	0.55	0.65	0.72	0.59
MgO	16.65	15.66	15.38	15.61	14.85	15.20	14.53	16.86	16.65	15.85	15.70	15.56	15.62	16.23	14.40
CaO	21.82	21.92	20.98	21.65	21.83	22.08	22.58	22.93	21.74	22.56	22.15	21.50	22.49	21.85	22.46
MnO	0.10	0.11	0.12	0.11	0.13	0.15	0.10	0.06	0.12	0.09	0.12	0.15	0.12	0.14	0.08
FeO	5.08	5.15	5.80	5.66	6.11	5.59	5.56	3.67	5.08	5.00	4.66	6.02	5.43	4.88	5.75
NiO	0.04	0.05	0.05	0.03	0.07	0.03	0.06	0.04	0.07	0.04	0.05	0.04	0.03	0.06	0.04
ZnO	0.00	0.00	0.00	0.00	0.00	0.00	0.00	0.00	0.00	0.00	0.00	0.00	0.00	0.00	0.00
Na_2O	0.19	0.29	0.27	0.23	0.22	0.32	0.26	0.21	0.27	0.27	0.34	0.30	0.23	0.29	0.27
K_2O	0.00	0.00	0.00	0.01	0.00	0.00	0.00	0.00	0.00	0.00	0.00	0.01	0.01	0.00	0.00
Total	100.18	100.58	99.12	99.89	98.92	101.18	100.05	100.00	100.24	100.53	100.03	100.13	100.98	99.82	99.19
Si	1.95	1.94	1.97	1.96	1.93	1.92	1.92	1.97	1.95	1.94	1.96	1.95	1.94	1.95	1.96
Ti	0.02	0.03	0.03	0.03	0.03	0.04	0.04	0.02	0.02	0.03	0.02	0.03	0.03	0.02	0.03
Al	0.07	0.11	0.08	0.08	0.10	0.12	0.11	0.05	0.07	0.08	0.07	0.08	0.09	0.07	0.08
Cr	0.02	0.02	0.02	0.02	0.01	0.03	0.03	0.02	0.02	0.03	0.03	0.02	0.02	0.02	0.02
Fe3+	0.00	0.00	0.00	0.00	0.00	0.00	0.00	0.00	0.00	0.00	0.00	0.00	0.00	0.00	0.00
Mg	0.91	0.85	0.85	0.86	0.83	0.83	0.80	0.92	0.91	0.87	0.86	0.85	0.85	0.89	0.80
Ca	0.85	0.85	0.82	0.84	0.86	0.85	0.88	0.89	0.84	0.87	0.86	0.84	0.87	0.85	0.88
Mn	0.00	0.00	0.00	0.00	0.00	0.00	0.00	0.00	0.00	0.00	0.00	0.00	0.00	0.00	0.00
Fe2+	0.16	0.16	0.18	0.17	0.19	0.17	0.17	0.11	0.16	0.15	0.14	0.19	0.17	0.15	0.18
Ni	0.00	0.00	0.00	0.00	0.00	0.00	0.00	0.00	0.00	0.00	0.00	0.00	0.00	0.00	0.00
Na	0.01	0.02	0.02	0.02	0.02	0.02	0.02	0.01	0.02	0.02	0.02	0.02	0.02	0.02	0.02
$Mg^{\#}$	85.39	84.42	82.55	83.10	81.24	82.89	82.32	89.11	85.38	84.98	85.73	82.16	83.68	85.58	81.70
En	47.60	45.91	45.88	45.72	43.97	44.70	43.15	47.91	47.67	45.73	46.14	45.51	45.11	47.08	42.91
Fs	8.15	8.47	9.70	9.30	10.16	9.22	9.27	5.85	8.16	8.08	7.68	9.88	8.80	7.94	9.61
Wo	44.26	45.62	44.42	44.99	45.87	46.08	47.58	46.24	44.16	46.19	46.18	44.61	46.09	44.99	47.48

Sample	DT1413	DT1413	DT1413	DT1414	DT1414	DT1414	DT1414	DT1414	DT1414	DT1414	DT1414	DT1403	DT1406	DT1406
Group	Pic	Pic	Pic	Pic	Pic	Pic	Pic	Pic	Pic	Pic	Pic	I	I	I
SiO_2	52.35	52.38	53.41	52.51	52.70	52.34	51.70	52.25	53.22	51.49	52.06	49.91	50.79	49.54
TiO_2	1.24	0.90	0.98	0.99	1.36	0.87	1.44	0.99	0.82	1.51	1.24	2.16	1.06	1.29
Al_2O_3	2.07	1.39	1.77	1.74	2.25	2.13	3.13	1.90	1.38	3.45	2.16	4.94	4.25	4.97

Table 5 continued

Sample	DT1413	DT1413	DT1413	DT1414	DT1414	DT1414	DT1414	DT1414	DT1414	DT1414	DT1414	DT1403	DT1406	DT1406
Group	Pic	Pic	Pic	Pic	Pic	Pic	Pic	Pic	Pic	Pic	Pic	I	I	I
Cr_2O_3	0.64	0.28	0.76	0.76	0.44	1.15	1.17	0.58	0.88	0.60	0.62	0.02	0.28	0.03
MgO	15.27	15.16	15.49	16.48	15.11	16.05	15.31	15.73	15.52	14.72	15.75	14.19	15.49	14.86
CaO	22.14	22.96	22.81	21.34	22.39	21.60	21.13	21.80	22.91	21.97	22.27	18.15	19.52	18.64
MnO	0.12	0.08	0.10	0.13	0.10	0.09	0.13	0.12	0.08	0.13	0.09	0.30	0.14	0.18
FeO	5.88	4.66	4.99	5.47	5.90	4.69	5.83	5.29	4.19	6.75	5.86	11.55	7.23	8.63
NiO	0.04	0.06	0.04	0.05	0.04	0.05	0.04	0.03	0.04	0.05	0.03	0.00	0.04	0.00
ZnO	0.00	0.00	0.00	0.00	0.00	0.00	0.00	0.00	0.00	0.00	0.00	0.00	0.00	0.00
Na_2O	0.26	0.22	0.26	0.28	0.28	0.36	0.37	0.25	0.28	0.47	0.24	0.32	0.22	0.26
K_2O	0.00	0.00	0.00	0.00	0.01	0.00	0.00	0.00	0.00	0.01	0.02	0.00	0.00	0.01
Total	100.00	98.09	100.62	99.74	100.58	99.33	100.25	98.93	99.31	101.14	100.32	101.54	99.01	98.40
Si	1.93	1.96	1.95	1.94	1.93	1.94	1.90	1.94	1.97	1.89	1.92	1.84	1.89	1.87
Ti	0.03	0.03	0.03	0.03	0.04	0.02	0.04	0.03	0.02	0.04	0.03	0.06	0.03	0.04
Al	0.09	0.06	0.08	0.08	0.10	0.09	0.14	0.08	0.06	0.15	0.09	0.22	0.19	0.22
Cr	0.02	0.01	0.02	0.02	0.01	0.03	0.03	0.02	0.03	0.02	0.02	0.00	0.01	0.00
Fe3+	0.00	0.00	0.00	0.00	0.00	0.00	0.00	0.00	0.00	0.00	0.00	0.00	0.00	0.00
Mg	0.84	0.85	0.84	0.91	0.83	0.88	0.84	0.87	0.85	0.81	0.87	0.78	0.86	0.83
Ca	0.86	0.91	0.88	0.83	0.87	0.84	0.82	0.86	0.90	0.85	0.87	0.71	0.77	0.74
Mn	0.00	0.00	0.00	0.00	0.00	0.00	0.00	0.00	0.00	0.00	0.00	0.01	0.00	0.01
Fe2+	0.18	0.15	0.15	0.17	0.18	0.15	0.18	0.16	0.13	0.21	0.18	0.36	0.23	0.27
Ni	0.00	0.00	0.00	0.00	0.00	0.00	0.00	0.00	0.00	0.00	0.00	0.00	0.00	0.00
Na	0.02	0.02	0.02	0.02	0.02	0.03	0.03	0.02	0.02	0.03	0.02	0.02	0.02	0.02
$Mg^{\#}$	82.24	85.29	84.70	84.29	82.03	85.91	82.39	84.11	86.86	79.54	82.73	68.66	79.25	75.42
En	44.55	44.50	44.93	47.50	44.05	47.19	45.59	46.03	45.48	43.16	45.20	42.31	46.38	45.13
Fs	9.62	7.67	8.11	8.85	9.65	7.74	9.75	8.69	6.88	11.10	9.43	19.31	12.15	14.70
Wo	45.83	47.82	46.96	43.65	46.30	45.07	44.66	45.27	47.64	45.73	45.36	38.38	41.48	40.16

Sample	DT1406	DT1406	DT1406	DT1406	DT1406	DT1406	DT1406	DT1406	DT1406	DT1406	DT1407	DT1407	DT1407	DT1407
Group	I	I	I	I	I	I	I	I	I	I	I	I	I	I
SiO_2	50.86	49.53	49.85	50.69	51.70	49.39	48.21	48.40	49.19	50.98	51.19	51.87	50.32	51.52
TiO_2	1.16	1.61	1.20	1.18	0.76	1.24	1.75	1.71	1.79	1.28	1.38	0.89	1.21	1.30
Al_2O_3	4.24	5.26	4.40	4.67	3.07	5.11	5.09	5.32	6.26	4.25	4.28	3.02	3.90	3.86
Cr_2O_3	0.35	0.27	0.07	0.21	0.55	0.12	0.01	0.02	0.17	0.48	0.47	0.31	0.10	0.77
MgO	16.53	14.78	15.85	15.22	17.01	15.33	13.44	14.18	14.23	15.32	16.92	16.08	15.82	16.73
CaO	17.25	19.86	16.35	19.61	18.07	18.66	18.91	18.37	20.00	20.27	16.71	19.53	19.77	18.85
MnO	0.20	0.18	0.24	0.19	0.20	0.19	0.21	0.18	0.18	0.19	0.16	0.18	0.17	0.15

Table 5 continued

Sample	DT1406	DT1406	DT1406	DT1406	DT1406	DT1406	DT1406	DT1406	DT1406	DT1406	DT1407	DT1407	DT1407	DT1407
Group	I	I	I	I	I	I	I	I	I	I	I	I	I	I
FeO	8.32	7.59	9.60	7.70	7.11	8.25	10.25	9.58	8.04	7.18	6.98	6.85	7.33	6.62
NiO	0.04	0.00	0.03	0.02	0.03	0.01	0.00	0.03	0.05	0.03	0.05	0.06	0.04	0.04
ZnO	0.00	0.00	0.00	0.00	0.00	0.00	0.00	0.00	0.00	0.00	0.00	0.00	0.00	0.00
Na_2O	0.21	0.28	0.30	0.35	0.25	0.28	0.36	0.26	0.29	0.25	0.21	0.25	0.26	0.22
K_2O	0.00	0.00	0.01	0.00	0.01	0.00	0.00	0.00	0.00	0.01	0.00	0.00	0.01	0.00
Total	99.15	99.35	97.90	99.83	98.77	98.58	98.23	98.05	100.19	100.24	98.36	99.03	98.93	100.08
Si	1.89	1.85	1.88	1.88	1.92	1.85	1.84	1.84	1.82	1.88	1.90	1.93	1.88	1.89
Ti	0.03	0.05	0.03	0.03	0.02	0.03	0.05	0.05	0.05	0.04	0.04	0.02	0.03	0.04
Al	0.19	0.23	0.20	0.20	0.13	0.23	0.23	0.24	0.27	0.18	0.19	0.13	0.17	0.17
Cr	0.01	0.01	0.00	0.01	0.02	0.00	0.00	0.00	0.00	0.01	0.01	0.01	0.00	0.02
Fe3+	0.00	0.00	0.00	0.00	0.00	0.00	0.00	0.00	0.00	0.00	0.00	0.00	0.00	0.00
Mg	0.91	0.82	0.89	0.84	0.94	0.86	0.76	0.80	0.79	0.84	0.94	0.89	0.88	0.92
Ca	0.68	0.78	0.65	0.77	0.71	0.74	0.76	0.74	0.78	0.79	0.66	0.77	0.78	0.73
Mn	0.01	0.01	0.01	0.01	0.01	0.01	0.01	0.01	0.01	0.01	0.01	0.01	0.01	0.00
Fe2+	0.26	0.24	0.30	0.24	0.22	0.26	0.33	0.30	0.25	0.22	0.22	0.21	0.23	0.20
Ni	0.00	0.00	0.00	0.00	0.00	0.00	0.00	0.00	0.00	0.00	0.00	0.00	0.00	0.00
Na	0.02	0.02	0.02	0.02	0.02	0.02	0.03	0.02	0.02	0.02	0.02	0.02	0.02	0.02
$Mg^{\#}$	77.97	77.64	74.65	77.88	81.00	76.82	70.03	72.52	75.92	79.19	81.21	80.70	79.36	81.83
En	49.43	44.61	48.27	45.48	50.28	46.18	41.22	43.51	43.21	45.42	51.77	47.60	46.57	49.47
Fs	13.96	12.85	16.39	12.92	11.80	13.93	17.64	16.49	13.70	11.93	11.97	11.38	12.11	10.98
Wo	36.61	42.54	35.33	41.60	37.92	39.89	41.14	40.00	43.09	42.65	36.26	41.02	41.32	39.55
Sample	DT1407	11DT03	11DT03	11DT03	11DT03	11DT03	11DT03	11DT03	11DT03	DT1205	DT1205	DT1205	DT1205	DT1205
Group	I	II	II	II	II	II	II	II	II	II	II	II	II	II
SiO_2	49.67	52.46	52.63	51.52	53.10	51.66	53.82	52.70	52.07	51.87	51.31	51.43	52.47	50.86
TiO_2	1.60	0.37	0.30	0.32	0.40	0.74	0.10	0.58	1.15	0.30	0.18	0.27	0.22	0.25
Al_2O_3	4.77	2.05	1.38	1.85	1.87	2.77	1.28	2.32	3.09	1.16	0.94	1.20	1.07	1.09
Cr_2O_3	0.03	0.16	0.16	0.13	0.18	0.17	0.07	0.21	0.22	0.12	0.17	0.17	0.14	0.22
MgO	15.30	13.14	13.64	12.79	13.11	12.94	13.57	13.41	13.14	11.63	12.38	12.67	12.61	12.68
CaO	19.20	22.79	23.69	23.30	22.98	22.60	23.34	22.95	22.69	22.22	22.57	22.80	22.22	22.50
MnO	0.19	0.23	0.24	0.22	0.26	0.24	0.24	0.19	0.22	0.20	0.18	0.19	0.22	0.20
FeO	8.77	9.28	7.96	8.68	8.80	8.84	8.25	7.97	8.38	10.05	9.53	9.83	10.27	10.07
NiO	0.05	0.00	0.01	0.02	0.01	0.01	0.00	0.00	0.01	0.02	0.00	0.03	0.00	0.02
ZnO	0.00	0.00	0.00	0.00	0.00	0.00	0.00	0.00	0.00	0.00	0.00	0.00	0.00	0.00
Na_2O	0.30	0.25	0.21	0.27	0.26	0.25	0.22	0.21	0.24	0.19	0.19	0.20	0.18	0.16

Table 5 continued

Sample	DT1407	11DT03	11DT03	11DT03	11DT03	11DT03	11DT03	11DT03	11DT03	DT1205	DT1205	DT1205	DT1205	DT1205
Group	I	II	II	II	II	II	II	II	II	II	II	II	II	II
K_2O	0.00	0.00	0.00	0.02	0.00	0.00	0.01	0.00	0.00	0.00	0.01	0.00	0.00	0.00
Total	99.88	100.72	100.23	99.12	100.97	100.21	100.89	100.54	101.21	97.75	97.45	98.77	99.40	98.05
Si	1.85	1.95	1.96	1.95	1.97	1.93	1.99	1.95	1.92	2.00	1.98	1.96	1.99	1.96
Ti	0.04	0.01	0.01	0.01	0.01	0.02	0.00	0.02	0.03	0.01	0.01	0.01	0.01	0.01
Al	0.21	0.09	0.06	0.08	0.08	0.12	0.06	0.10	0.13	0.05	0.04	0.05	0.05	0.05
Cr	0.00	0.00	0.00	0.00	0.01	0.00	0.00	0.01	0.01	0.00	0.01	0.01	0.00	0.01
Fe3+	0.00	0.00	0.00	0.00	0.00	0.00	0.00	0.00	0.00	0.00	0.00	0.00	0.00	0.00
Mg	0.85	0.73	0.76	0.72	0.72	0.72	0.75	0.74	0.72	0.67	0.71	0.72	0.71	0.73
Ca	0.76	0.90	0.93	0.93	0.90	0.89	0.91	0.90	0.89	0.90	0.92	0.92	0.89	0.92
Mn	0.01	0.01	0.01	0.01	0.01	0.01	0.01	0.01	0.01	0.01	0.01	0.01	0.01	0.01
Fe2+	0.27	0.29	0.25	0.27	0.27	0.28	0.26	0.25	0.26	0.32	0.31	0.31	0.33	0.32
Ni	0.00	0.00	0.00	0.00	0.00	0.00	0.00	0.00	0.00	0.00	0.00	0.00	0.00	0.00
Na	0.02	0.02	0.02	0.02	0.02	0.02	0.02	0.01	0.02	0.01	0.01	0.01	0.01	0.01
$Mg^{\#}$	75.66	71.62	75.33	72.42	72.64	72.31	74.56	75.00	73.65	67.35	69.85	69.67	68.63	69.18
En	45.20	38.06	39.07	37.40	38.17	38.14	39.04	39.26	38.72	35.20	36.69	36.87	36.93	36.97
Fs	14.54	15.09	12.79	14.24	14.37	14.61	13.32	13.09	13.85	17.06	15.84	16.05	16.88	16.47
Wo	40.26	46.85	48.13	48.36	47.46	47.26	47.64	47.65	47.43	47.74	47.47	47.08	46.19	46.55
Sample	DT1205	DT1205	DT1205	DT1205	DT1411	DT1411	DT1411	DT1411	DT1411	DT1411	DT1411	DT1411	DT1411	DT1411
Group	II	II	II	II	II	II	II	II	II	II	II	II	II	II
SiO_2	51.82	52.20	52.37	53.14	50.02	50.12	51.56	48.83	48.79	51.82	49.51	50.21	48.51	49.33
TiO_2	0.33	0.35	0.25	0.18	2.24	2.21	1.41	2.63	1.75	1.18	2.26	2.52	2.58	2.70
Al_2O_3	1.17	1.17	1.15	1.03	3.55	3.34	1.65	4.03	2.40	1.39	3.29	3.65	3.84	3.74
Cr_2O_3	0.16	0.13	0.12	0.08	0.37	0.26	0.11	0.43	0.02	0.02	0.24	0.26	0.41	0.43
MgO	12.61	12.74	12.67	12.98	12.84	12.97	13.10	12.26	11.47	12.79	12.42	12.43	12.44	11.92
CaO	22.04	22.15	22.44	22.98	20.23	19.53	19.14	21.01	18.81	16.89	19.86	19.79	19.96	20.46
MnO	0.22	0.18	0.21	0.21	0.27	0.26	0.31	0.22	0.34	0.42	0.27	0.29	0.28	0.23
FeO	10.61	10.63	10.13	9.85	10.86	11.81	13.01	9.95	15.37	16.23	11.69	12.04	11.03	11.35
NiO	0.01	0.04	0.00	0.00	0.01	0.02	0.01	0.03	0.00	0.00	0.00	0.00	0.02	0.02
ZnO	0.00	0.00	0.00	0.00	0.00	0.00	0.00	0.00	0.00	0.00	0.00	0.00	0.00	0.00
Na_2O	0.23	0.17	0.21	0.23	0.30	0.30	0.27	0.25	0.27	0.17	0.26	0.29	0.27	0.22
K_2O	0.00	0.00	0.00	0.00	0.00	0.00	0.00	0.00	0.00	0.01	0.01	0.00	0.01	0.00
Total	99.20	99.75	99.55	100.68	100.69	100.81	100.56	99.65	99.22	100.90	99.81	101.47	99.33	100.41
Si	1.97	1.97	1.98	1.98	1.87	1.88	1.94	1.85	1.89	1.96	1.88	1.87	1.85	1.86
Ti	0.01	0.01	0.01	0.01	0.06	0.06	0.04	0.07	0.05	0.03	0.06	0.07	0.07	0.08

Table 5 continued

Sample	DT1205	DT1205	DT1205	DT1205	DT1411	DT1411	DT1411	DT1411	DT1411	DT1411	DT1411	DT1411	DT1411	DT1411
Group	II	II	II	II	II	II	II	II	II	II	II	II	II	II
Al	0.05	0.05	0.05	0.05	0.16	0.15	0.07	0.18	0.11	0.06	0.15	0.16	0.17	0.17
Cr	0.00	0.00	0.00	0.00	0.01	0.01	0.00	0.01	0.00	0.00	0.01	0.01	0.01	0.01
Fe3+	0.00	0.00	0.00	0.00	0.00	0.00	0.00	0.00	0.00	0.00	0.00	0.00	0.00	0.00
Mg	0.71	0.72	0.71	0.72	0.72	0.72	0.73	0.69	0.66	0.72	0.70	0.69	0.71	0.67
Ca	0.89	0.89	0.90	0.91	0.80	0.77	0.76	0.84	0.77	0.67	0.80	0.78	0.80	0.82
Mn	0.01	0.01	0.01	0.01	0.01	0.01	0.01	0.01	0.01	0.01	0.01	0.01	0.01	0.01
Fe2+	0.34	0.34	0.32	0.31	0.34	0.37	0.41	0.31	0.50	0.51	0.37	0.38	0.35	0.36
Ni	0.00	0.00	0.00	0.00	0.00	0.00	0.00	0.00	0.00	0.00	0.00	0.00	0.00	0.00
Na	0.02	0.01	0.02	0.02	0.02	0.02	0.02	0.02	0.02	0.01	0.02	0.02	0.02	0.02
$Mg^{\#}$	67.94	68.11	69.03	70.14	67.82	66.19	64.21	68.70	57.08	58.42	65.45	64.79	66.79	65.17
En	36.88	37.02	36.96	37.29	38.57	38.77	38.55	37.42	34.30	37.75	37.56	37.40	37.94	36.33
Fs	17.40	17.33	16.58	15.88	18.30	19.80	21.48	17.05	25.78	26.87	19.83	20.32	18.86	19.42
Wo	45.73	45.65	46.46	46.83	43.12	41.43	39.97	45.53	39.92	35.38	42.61	42.27	43.19	44.25

Sample	DT1412	DT1412	DT1412	DT1412	DT1412	DT1412	DT1412
Group	II	II	II	II	II	II	II
SiO_2	49.62	50.49	49.93	48.38	50.04	50.39	50.20
TiO_2	2.11	1.97	2.29	2.10	1.69	2.11	2.37
Al_2O_3	2.92	2.39	3.37	4.28	2.52	3.38	3.63
Cr_2O_3	0.00	0.17	0.36	0.35	0.02	0.21	0.33
MgO	11.41	12.77	12.38	11.80	11.29	12.91	12.09
CaO	19.60	20.14	20.22	19.32	19.23	20.64	21.07
MnO	0.34	0.27	0.28	0.28	0.33	0.23	0.25
FeO	14.50	11.67	11.71	11.37	14.76	11.04	11.06
NiO	0.01	0.02	0.00	0.01	0.00	0.00	0.01
ZnO	0.00	0.00	0.00	0.00	0.00	0.00	0.00
Na_2O	0.33	0.29	0.29	0.32	0.24	0.30	0.29
K_2O	0.01	0.00	0.01	0.01	0.00	0.00	0.00
Total	100.85	100.17	100.84	98.20	100.11	101.22	101.29
Si	1.88	1.91	1.87	1.86	1.91	1.88	1.87
Ti	0.06	0.06	0.06	0.06	0.05	0.06	0.07
Al	0.13	0.11	0.15	0.19	0.11	0.15	0.16
Cr	0.00	0.00	0.01	0.01	0.00	0.01	0.01
Fe3+	0.00	0.00	0.00	0.00	0.00	0.00	0.00
Mg	0.65	0.72	0.69	0.68	0.64	0.72	0.67

Table 5 continued

Sample	DT1412	DT1412	DT1412	DT1412	DT1412	DT1412	DT1412
Group	II	II	II	II	II	II	II
Ca	0.79	0.80	0.80	0.79	0.78	0.81	0.83
Mn	0.01	0.01	0.01	0.01	0.01	0.01	0.01
Fe2+	0.46	0.37	0.37	0.37	0.47	0.34	0.34
Ni	0.00	0.00	0.00	0.00	0.00	0.00	0.00
Na	0.02	0.02	0.02	0.02	0.02	0.02	0.02
$Mg^{\#}$	58.38	66.10	65.33	64.90	57.69	67.57	66.08
En	34.11	38.00	37.18	36.99	33.98	38.25	36.36
Fs	24.32	19.48	19.73	20.01	24.93	18.36	18.66
Wo	41.57	42.52	43.09	43.00	41.09	43.40	44.98

$Mg^{\#} = 100 \times (MgO/(MgO + FeO))$, molar

Pic picritic rocks

References

Adam J, Green T (2006) Trace element partitioning between mica- and amphibole-bearing garnet lherzolite and hydrous basanitic melt: 1. Experimental results and the investigation of controls on partitioning behaviour. Contrib Mineral Petrol 152:1–17

Albaredè F (1992) How deep do common basalts form and differentiate? J Geophys Res 97:10997–11009

Blundy JD, Robinson JAC, Wood BJ (1998) Heavy REE are compatible in clinopyroxene on the spinel lherzolite solidus. Earth Planet Sci Lett 160:493–504

Bogdanova SV, Pisarevsky SA, Li ZX (2009) Assembly and breakup of Rodinia (some results of IGCP project 440). Stratigr Geol Correl 17:259–274

Boynton WV (1984) Geochemistry of the rare earth elements: meteorite studies. In: Henderson P (ed) Rare earth element geochemistry. Elsevier, Amsterdam, pp 63–114

Cong BL (ed) (1988) Formation and evolution of Panxi paleo-rift. Science Press, Beijing **(in Chinese)**

Ernst RE, Wingate MTD, Buchan KL et al (2008) Global record of 1600–700 Ma large igneous provinces (LIPS): implications for the reconstruction of the proposed Nuna (Columbia) and Rodinia supercontinents. Precambrian Res 160:159–178

Evans DAD (2013) Reconstructing pre-Pangean supercontinents. Geol Soc Am Bull 125:1735–1751

Ghiorso MS, Sack RO (1995) Chemical mass transfer in magmatic processes IV. A revised and internally consistent thermodynamic model for the interpolation and extrapolation of liquid–solid equilibria in magmatic systems at elevated temperatures and pressures. Contrib Mineral Petrol 119:197–212

Giret A, Lameyre J (1985) Inverted alkaline–tholeiitic sequences related to lithospheric thickness in the evolution of continental rifts and oceanic islands. J Afr Earth Sci 3(1–2):261–268

Greentree MR, Li ZX (2008) The oldest known rocks in south-western China: SHRIMP U–Pb magmatic crystallization age and detrital provenance analysis of the Paleoproterozoic Dahongshan Group. J Asian Earth Sci 33:289–302

Greentree MR, Li ZX, Li XH (2006) Latest Mesoproterozoic to earliest Neoproterozoic basin record of the Sibao orogenesis in western South China and relationship to the assembly of Rodinia. Precambrian Res 151:79–100

Griffin WL, O'Reilly SY, Afonso JC et al (2009) The composition and evolution of lithospheric mantle: a re-evaluation and its tectonic implications. J Petrol 50:1185–1204

He DF (2009) Petrological and geochemical characteristics of the Lala copper deposit in Sichuan Province. The Gradute School of the Chinese Academy of Sciences, China **(in Chinese with English abstract)**

Hofmann AW, White WM (1982) Mantle plumes from ancient oceanic crust. Earth Planet Sci Lett 57:421–436

Johnson KTM (1998) Experimental determination of partition coefficients for rare earth and high-field-strength elements between clinopyroxene, garnet, and basaltic melt at high pressures. Contrib Mineral Petrol 133:60–68

Keays RR (1995) The role of komatiitic and picritic magmatism and S-saturation in the formation of ore deposits. Lithos 34:1–18

Kinzler RJ (1997) Melting of mantle peridotite at pressures approaching the spinel to garnet transition: application to mid-ocean ridge basalt petrogenesis. J Geophys Res 102:853–874

Kullerud K, Skjerlie KP, Corfu F et al (2006) The 2.4 Ga Ringvassoy mafic dykes, West Trom Basement complex, Norway: the concluding act of early Palaeoproterozoic continental breakup. Precambrian Res 150:183–200

Li ZX, Zhang LH, Powell CM (1995) South China in Rodinia: Part of the missing link between Australia–East Antarctica and Laurentia? Geology 23:407–410

Li ZX, Li XH, Kinny PD et al (1999) The breakup of Rodinia: Did it start with a mantle plume beneath South China? Earth Planet Sci Lett 173:171–181

Li XH, Li ZX, Zhou H (2002a) U–Pb zircon geochronology, geochemistry and Nd isotopic study of Neoproterozoic bimodal volcanic rocks in the Kangding Rift of South China: implications for the initial rifting of Rodinia. Precambrian Res 113:135–155

Li ZX, Li XH, Zhou H et al (2002b) Grenville-aged continental collision in South China: new SHRIMP U–Pb zircon results and implications for Rodinia configuration. Geology 30:163–166

Li XH, Li ZX, Ge W et al (2003a) Neoproterozoic granitoids in South China: Crustal melting above a mantle plume at ca. 825 Ma? Precambrian Res 122:45–83

Li ZX, Li XH, Kinny PD et al (2003b) Geochronology of Neoproterozoic syn-rift magmatism in the Yangtze Craton, South China and correlations with other continents: evidence for a mantle superplume that broke up Rodinia. Precambrian Res 122:85–109

Li XH, Li ZX, Sinclair JA et al (2006) Revisiting the "Yanbian Terrane": implications for Neoproterozoic tectonic evolution of the western Yangtze Block, South China. Precambrian Res 151:14–30

Li ZX, Bogdanova SV, Collins AS et al (2008) Assembly, configuration, and break-up history of Rodinia: a synthesis. Precambrian Res 160:179–210

Li XH, Liu Y, Li QL et al (2009) Precise determination of Phanerozoic zircon Pb/Pb age by multi-collector SIMS without external standardization. Geochem Geophy Geosyst 10:Q04010

Li QL, Li XH, Liu Y et al (2010) Precise U–Pb and Pb–Pb dating of Phanerozoic baddeleyite by SIMS with oxygen flooding technique. J Anal Atom Spectrom 25:1107–1113

Lin GC, Li XH, Li WX (2007) SHRIMP U–Pb zircon age, geochemistry and Nd–Hf isotope of Neoproterozoic mafic dyke swarms in western Sichuan: petrogenesis and tectonic significance. Sci China Ser D 50:1–16

Ling WL, Gao S, Zhang BR et al (2003) Neoproterozoic tectonic evolution of the northwestern Yangtze craton, South China: implications for amalgamation and break-up of the Rodinia Supercontinent. Precambrian Res 122:111–140

Loucks RR (1990) Discrimination of ophiolitic from nonophiolitic ultramafic–mafic allochthons in orogenic belts by the Al/Ti ratio in clinopyroxene. Geology 18:346–349

Lugmair GW, Harti K (1978) Lunar initial $^{143}Nd/^{144}Nd$: differential evolution of the lunar crust and mantle. Earth Planet Sci Lett 39:349–357

McKenzie D, O'Nions RK (1991) Partial melt distributions from inversion of rare earth element concentrations. J Petrol 32:1021–1091

Naldrett AJ (2010) Secular variation of magmatic sulfide deposits and their source magmas. Econ Geol 105:669–688

Nance RD, Murphy JB, Santosh M (2014) The supercontinent cycle: a retrospective essay. Gondwana Res 25:4–29

Pearce JA, Cann JR (1973) Tectonic setting of basic volcanic rocks determined using trace element analysis. Earth Planet Sci Lett 19:290–300

Peate DW, Hawkesworth CJ, Mantovani MSM (1992) Chemical stratigraphy of the Parana lavas South America: classification of magma-types and their spatial distribution. Bull Volcanol 55:119–139

Qi L, Hu J, Grégoire DC (2000) Determination of trace elements in granites by inductively coupled plasma mass spectrometry. Talanta 51:507–513

Roeder PL, Emslie RF (1970) Olivine-liquid equilibrium. Contrib Mineral Petrol 29:275–289

Salter MJV, Stracke A (2004) Composition of the depleted mantle. Geochem Geophy Geosyst 5(5):1–27

Sharma M (1997) Siberian traps. In: Mahoney JJ, Coffin MF (eds) Large igneous provinces: continental, oceanic and planetary flood volcanism. American Geophysical Union Geophysical Monograph, New York, pp 273–295

Shaw DM (1970) Trace element fractionation during anatexis. Geochim Cosmochim Acta 34:237–243

Shervais JW (1982) Ti–V plots and the petrogenesis of modern and ophiolitic lavas. Earth Planet Sci Lett 59:101–118

Sichuan Bureau of Geology and Mineral Resource (SBGMR) (1991) Regional Geology of Sichuan Province. Geol. Publ. House, Beijing, p 730 **(in Chinese with English abstract)**

Spaeth G, Hotten R, Peters M et al (1995) Mafic dykes in the Shackleton Range, Antarctica. Polarforschung 63(2/3):101–121

Sprung P, Schuth S, Münker C et al (2007) Intraplate volcanism in New Zealand: the role of fossil plume material and variable lithospheric properties. Contrib Mineral Petrol 153:669–687

Sun SS, McDonough WF (1989) Chemical and isotopic systematics of oceanic basalts: implications for mantle composition and processes. In: Saunders AD, Norry MJ (eds.) Magmatism in the Ocean Basins. Geological Society, London, Special Publications, no. 42, pp 313–345

Takahashi E, Kushiro I (1983) Melting of a dry peridotite at high pressures and basalt magma genesis. Am Mineral 68:859–879

Tang YJ, Zhang HF, Ying JF et al (2013) Widespread refertilization of cratonic and circum-cratonic lithospheric mantle. Earth Sci Rev 118:45–68

Taylor SR, McLennan SM (1995) The geochemical evolution of the continental crust. Rev Geophys 33:241–265

Van Westrenen W, Allan NL, Blundy JD et al (2000) Atomistic simulation of trace element incorporation into garnets-comparison with experimental garnet-melt partitioning data. Geochim Cosmochim Acta 64:1629–1639

Vermeesch P (2006) Tectonic discrimination diagrams revisited. Geochem Geophy Geosyst 7:Q06017. doi:10.1029/2005GC001092

Walter MJ (1998) Melting of garnet peridotite and the origin of komatiite and depleted lithosphere. J Petrol 39(1):29–60

Wang XC, Li XH, Li WX et al (2008) The Bikou basalts in northwestern Yangtze Block, South China: Remains of 820–800 Ma continental flood basalts? Geol Soc Am Bull 120:1478–1492

Wang YJ, Zhang AM, Peter A et al (2013) Geochronological, geochemical and Nd–Hf–Os isotopic fingerprinting of an early Neoproterozoic arc-back-arc system in South China and its accretionary assembly along the margin of Rodinia. Precambrian Res 231:343–371

Wang YJ, Zhang YZ, Fan WM et al (2014) Early Neoproterozoic accretionary assemblage in the Cathaysia Block: geochronological, Lu–Hf isotopic and geochemical evidence from granitoid gneisses. Precambrian Res 249:144–161

Wilson M (1989) Igneous petrogenesis. Chapman and Hall, London

Wilson M (1993) Geochemical characteristics of oceanic and continental basalts: A key to mantle dynamics? J Geol Soc Lond 150:977–990

Winchester JA, Floyd PA (1976) Geochemical magma type discrimination: application to altered and metamorphosed igneous rocks. Earth Planet Sci Lett 45:326–336

Wingate MTD, Compston W (2000) Crystal orientation effects during ion microprobe U–Pb analysis of baddeleyite. Chem Geol 168:75–97

Yang YJ, Bai ZJ, Zhu WG et al (2016) Platinum-group element geochemistry of the Neoproterozoic picritic dykes in the Panzhihua area, Sichuan Province. Bull Mineral Petrol Geochem 35(1):126–137 **(in Chinese with English abstract)**

Yunnan Bureau of Geology (YBG) (1972) A report of regional geological survey in Yongren area of the People's Republic of China (the scale of 1:200000) **(in Chinese)**

Zhao XF (2010) Paleoproterozoic crustal evolution and Fe–Cu metallogeny of the western Yangtze block, SW China. Unpublished Ph.D. thesis, University of Hong Kong, pp 1–192

Zhao JH, Zhou MF (2007a) Neoproterozoic adakitic plutons and arc magmatism along the western margins of the Yangtze Block, South China. J Geol 115:675–689

Zhao JH, Zhou MF (2007b) Geochemistry of Neoproterozoic mafic intrusions in the Panzhihua district (Sichuan Province, SW China): implications for subduction-related metasomatism in the upper mantle. Precambrian Res 152:27–47

Zhao JH, Zhou MF, Yan DP et al (2008) Zircon Lu–Hf isotopic constraints on Neoproterozoic subduction-related crustal growth along the western margin of the Yangtze Block, South China. Precambrian Res 163:189–209

Zhou MF, Kennedy AK, Sun M et al (2002a) Neoproterozoic arc-related mafic intrusions along the northern margin of South China: implications for the accretion of Rodinia. J Geol 110:611–618

Zhou MF, Yan DP, Kennedy AK et al (2002b) SHRIMP U–Pb zircon geochronological and geochemical evidence for Neoproterozoic arc-magmatism along the western margin of the Yangtze Block, South China. Earth Planet Sci Lett 196:51–67

Zhou MF, Ma YX, Yan DP et al (2006) The Yanbian terrane (southern Sichuan Province, SW China): a Neoproterozoic arc assemblage in the western margin of the Yangtze Block. Precambrian Res 144:19–38

Zhou JB, Li XH, Ge W et al (2007) Age and origin of middle Neoproterozoic mafic magmatism in southern Yangtze Block and relevance to the break-up of Rodinia. Gondwana Res 12:184–197

Zhu WG, Zhong H, Deng HL et al (2006) SHRIMP zircon U–Pb age, geochemistry and Nd–Sr isotopes of the Gaojiacun mafic–ultramafic intrusive complex, SW China. Int Geol Rev 48:650–668

Zhu WG, Zhong H, Li XH et al (2007) ^{40}Ar–^{39}Ar age, geochemistry and Sr–Nd–Pb isotopes of the Neoproterozoic Lengshuiqing Cu–Ni sulfide-bearing mafic–ultramafic complex, SW China. Precambrian Res 155:98–124

Zhu WG, Zhong H, Li XH et al (2008) SHRIMP Zircon U–Pb geochronology, elemental, and Nd isotopic geochemistry of the Neoproterozoic mafic dykes in the Yanbian area, SW China. Precambrian Res 164:66–85